FIG. 1. *L3/Lhx8* and *Lhx6* mRNAs are expressed in developing basal forebrain. The *L3/Lhx8* mRNA expression domain is included in that of *Lhx6*. (a) *L3/Lhx8* mRNA is expressed in the medial ganglionic eminence (MGE) and mesenchymal cells in the upper and lower jaws (JAWS). A sagittal section of the wild type (WT) E12.5 embryo was hybridized with an *L3/Lhx8* full-length probe. (b and c) The *L3/Lhx8* mRNA expression domain is included in that of *Lhx6* in the MGE and *L3/Lhx8* mRNA is expressed in a relatively more anterior part of the MGE than *Lhx6*. The scale bar in (a) represents 1 mm, also for (c). Serial sagittal sections of an E12.5 embryo were hybridized with an *L3/Lhx8* full-length probe (b) or *Lhx6* probe (c). (d–i) *L3/Lhx8* and *Lhx6* mRNAs are co-localized in the same cells in the MGE. Double-labelling fluorescence *in situ* hybridization was performed on the same coronal section of the E12.5 embryo; green, *L3/Lhx8* probe (c and g); red, *Lhx6* probe (e and h); and merged (f and i). Double-positive cells are yellow. Panels (g)–(i) are higher-magnification photographs of (d)–(f), respectively. The scale bar in (d) represents 50 μm, and for (e) and (f). The scale bar in (g) represents 25 μm, and for (h) and (i).
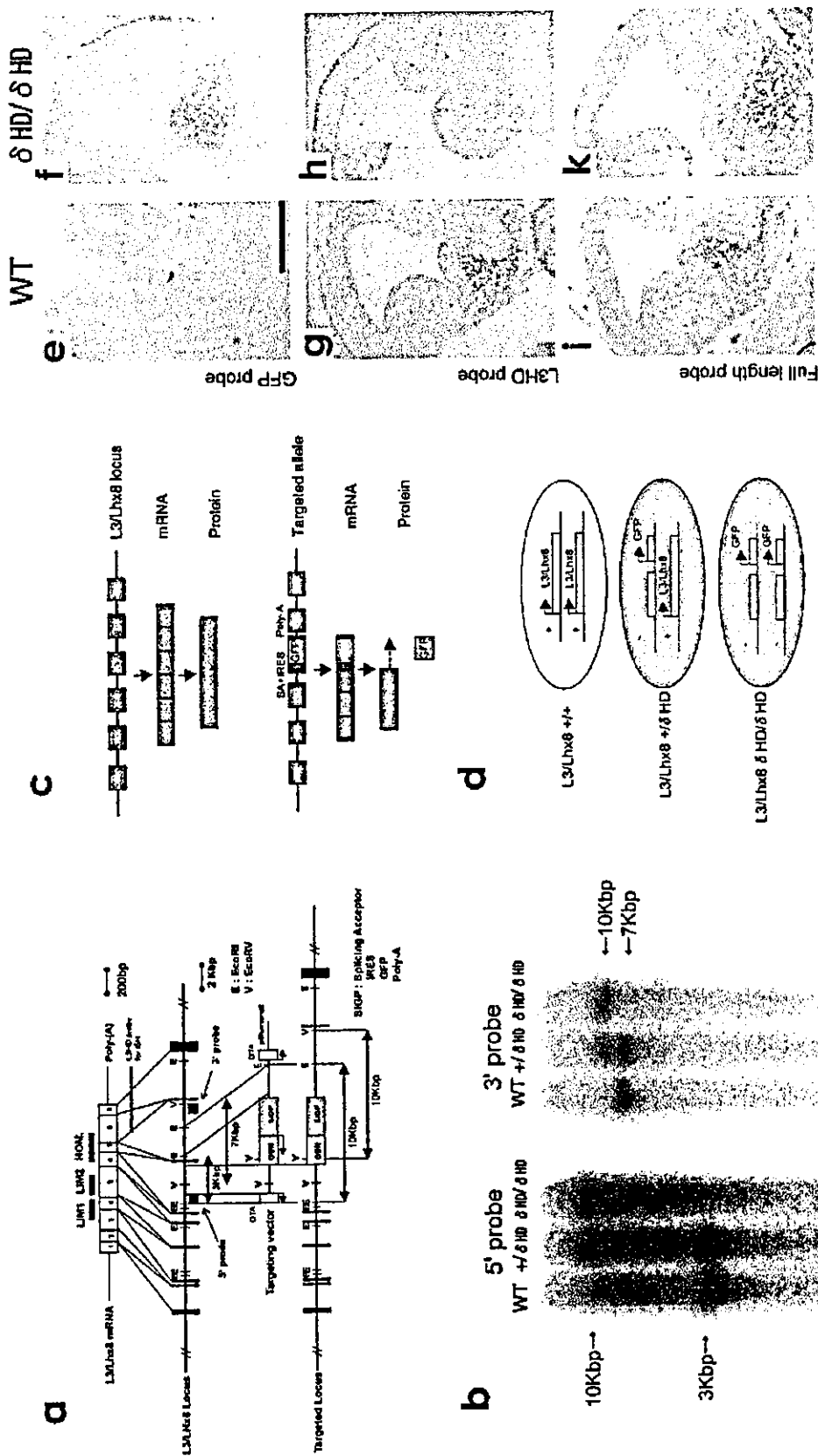
FIG. 2. *L3/Lhx8* targeting strategy and genotyping. (a) A restriction map of the genomic region containing *L3/Lhx8* is shown at the top with the relative positions of each exon. The targeting vector (middle) and the targeted locus (bottom) are also shown. (b) Genotyping of the embryos from the *L3/Lhx8+/δHD* intercross analysed by Southern blotting. *EcoRI-* (left) or *EcoRV-* (right) digested genomic DNAs were hybridized with an external 5' probe or 3' probe, respectively. The 5' probe recognizes the 3-kbp wild type allele and the 10-kbp targeted allele. The 3' probe recognizes the 7-kbp wild type allele and the 10-kbp targeted allele. RI, *EcoRI*; V, *EcoRV*; *NEO*, neomycin-resistant gene cassette; *SIGP, green fluorescent protein (GFP)* expression cassette (see Materials and methods and below). Fusion mRNA consisting of tandem LIM domains of *L3/Lhx8* and eGFP mRNAs is expressed from the targeted allele. (c) Scheme of eGFP protein expression from the *SIGP (Splicing acceptor + IRES + eGFP + PolyA signal)* cassette. Fusion mRNA with tandem LIM domains and eGFP would be transcribed by the splicing acceptor. From this fusion mRNA, LIM domain-only protein and, simultaneously, eGFP protein would be translated via *IRES*. (d) As a result, heterozygous and homozygous cells express *eGFP* from the targeted allele. eGFP mRNA is expressed in heterozygous (data not shown) and homozygous mice (f), but not in the WT mice (e). The homeodomain-specific (*L3HD*) probe does not label homozygous MGE (h), but does label WT (g) and heterozygous (data not shown) MGE. By contrast, the full-length probe of *L3/Lhx8* labels WT (i), heterozygous (data not shown) and homozygous (k) MGE. The scale bar in (c) represents 500 μm for all panels.

M-MLV RTase from 5 μg total RNA. PCR was performed with the primers described previously (Lopez-Coviella *et al.*, 2000).

Results

Characterization of L3/Lhx8 δHD mice

L3/Lhx8 mRNA was expressed in the medial ganglionic eminence (MGE) and the mesenchyme around the oral cavity (Matsumoto *et al.*, 1996; Zhao *et al.*, 1999) (Fig. 1a). *Lhx6* is closely related to *L3/Lhx8* and has a similar gene-expression profile; these two genes could have a redundant role in developing mice (Grigoriou *et al.*, 1998; Zhang *et al.*, 2002) (Fig. 1b and c). Double-labelling FISH indicated that their mRNAs were co-localized in the MGE (Fig. 1d–i). A notable point was that the *L3/Lhx8* mRNA expression domain was included within the *Lhx6* mRNA expression domain (Asbreuk *et al.*, 2002) (Fig. 1b–i). We therefore designed a targeting vector to disrupt the *L3/Lhx8* function and to limit simultaneously possible compensational effects of *Lhx6* (see Materials and methods, Fig. 2a)

Heterozygous (δHD/+) mice appeared normal and these animals mated to produce homozygous mutants. Progenies intercrossed between heterozygous mice were genotyped after weaning. We found that only 14 (3.76%) were δHD/δHD out of 372 offspring after weaning. Judging from the ratio of genotypes of embryos, δHD/δHD mutants were not embryonic lethal and so were born alive (Table 1). Their appearances and spontaneous motions were indistinguishable from WT and δHD/+ mice (data not shown), but most died within several hours, possibly due to a complete cleft of the secondary palate. The incidence rate of cleft palate among the δHD/δHD mutants was about 94% on postnatal day (P) 0; however, mutants without cleft palate (5.6%) could survive to adulthood (P30) (Table 1). The rate was clearly different from that (60%) of the previous −/− mice (Zhao *et al.*, 1999). Other craniofacial features of the δHD/δHD mutants (mandible, maxilla, teeth, tongue, etc.) appeared normal. The craniofacial phenotypes of the δHD/δHD mice will be described in detail elsewhere.

We could not detect an eGFP protein expression from targeted alleles under fluorescent microscopy or by immunohistochemistry with an anti-GFP antibody. Because *eGFP* mRNA expression was confirmed by ISH with an *eGFP* probe (Fig. 2f) and the expression pattern was similar to that of *L3/Lhx8* mRNA in WT mice (Fig. 2g and i), we speculate that the translation efficiency of *eGFP* is very low or it may be suppressed in the mice for some unknown reason. In the δHD/δHD mice, we could detect ISH signals with an *L3/Lhx8* full-length probe (Fig. 2j) but not with an HD probe (Fig. 2h). These results indicate that mRNA for the LIM domain of L3/Lhx8 protein is expressed from the targeted allele.

Molecular marker expression in the basal forebrain of δHD/δHD mice

To check whether patterning within the developing ventral telencephalon of δHD/δHD mice is altered, we compared expression patterns of several molecular markers between WT, δHD/+ and δHD/δHD mice by ISH histochemistry. The following probes were used as markers of the ventral telencephalon: *Dlx2* [ventricular zone (VZ) and subventricular zone (SVZ) of lateral and medial ganglionic eminence (LGE and MGE)] (Eisenstat *et al.*, 1999) (Fig. 3a and b); *Dlx5* (SVZ and mantle layer of LGE and MGE) (Eisenstat *et al.*, 1999) (Fig. 3c and d); *Nkx2.1* (whole MGE) (Marin *et al.*, 2002) (Fig. 3e and f); *Lhx6* (SVZ and mantle layer of MGE) (Grigoriou *et al.*, 1998; Kimura *et al.*, 1999) (Fig. 3g and h); and *Gbx2* (mantle layer of MGE) (Bulfone *et al.*, 1993) (Fig. 3i and j). In addition, *Shh* (mantle layer of MGE) (Kohtz *et al.*, 1998) (Fig. 3k and l) and its signalling components, *Ptc* (VZ most prominent in MGE) (Fig. 3m and n) and *Smo* (VZ) (Fig. 3o and p) mRNA expressions were examined, because Shh signalling is essential for the establishment of the ventral forebrain (Ericson *et al.*, 1995; Kohtz *et al.*, 1998). As illustrated in Fig. 3, none of the marker expression patterns changed in δHD/δHD mice as compared with WT or heterozygous mice.

Cholinergic neurons decreased in the basal forebrain of δHD/δHD mice

Because most BFCNs in adults express *L3/Lhx8* (Asbreuk *et al.*, 2002), we next examined several cholinergic marker expressions in δHD/δHD mice. At P0, we could not detect any cholinergic marker expressions in the basal forebrain; the markers included VAChT (Fig. 4e–h), p75 – a low-affinity NGF receptor (Fig. 4i–l), ChAT (data not shown) and choline transporter-1, CHT-1 (Misawa *et al.*, 2001) (data not shown). It should be noted that in other central nervous system regions, such as the spinal cord motor neurons, the marker expressions were similar between WT and δHD/δHD mice (Fig. 4m and n).

In the homozygous adults that survived (Table 1), we were able to detect ChAT-immunopositive cells in the basal forebrain, but the numbers were greatly diminished compared with WT or heterozygous mice (Fig. 5a–h). When we counted the cholinergic neurons per nuclei of the basal forebrain, the extent of the reduction varied between each nucleus in the homozygous mice as compared with WT mice (see Fig. 9). There are two possible explanations for this reduction: first, BFCNs of the homozygous mice died in a necrotic or apoptotic manner, and second, they changed their transmitter phenotype during development. We currently favour the latter hypothesis. The *GFP* mRNA expression pattern in the homozygous mice (Fig. 2f) was very similar to that of *L3/Lhx8* in the WT or heterozygous mice (Fig. 2i),

TABLE 1. *L3/Lhx8* δHD/δHD mice were not embryonic lethal

Stage	Total	WT (*n*)	WT (%)	+/δHD (*n*)	+/δHD (%)	δHD/δHD (*n*)	δHD/δHD (%)	δHD/δHD with cleft palate	δHD/δHD with normal palate
E12.5	88	31	35.2	39	44.3	18	20.5	–	–
E14.5	383	107	27.9	189	49.3	87	22.7	–	–
E16.5	57	16	28.1	27	47.4	14	24.6	–	–
E18.5	48	15	31.3	21	43.8	12	25.0	–	–
P0	178	50	28.1	75	42.1	53	29.8	50	3
P30	–	–	–	–	–	–	–	0	3

Heterozygous mice were intercrossed and their progenies genotyped at each stage. Homozygous embryos are present in the expected mendelian ratio of roughly 25% during the embryonic stage. Among 53 homozygous mice on P0, only three exhibit a normal palate and survive to adulthood (P30). The incidence of cleft palate among homozygous mice was about 94%. The morning of the appearance of the copulation plug was defined as E0.5.
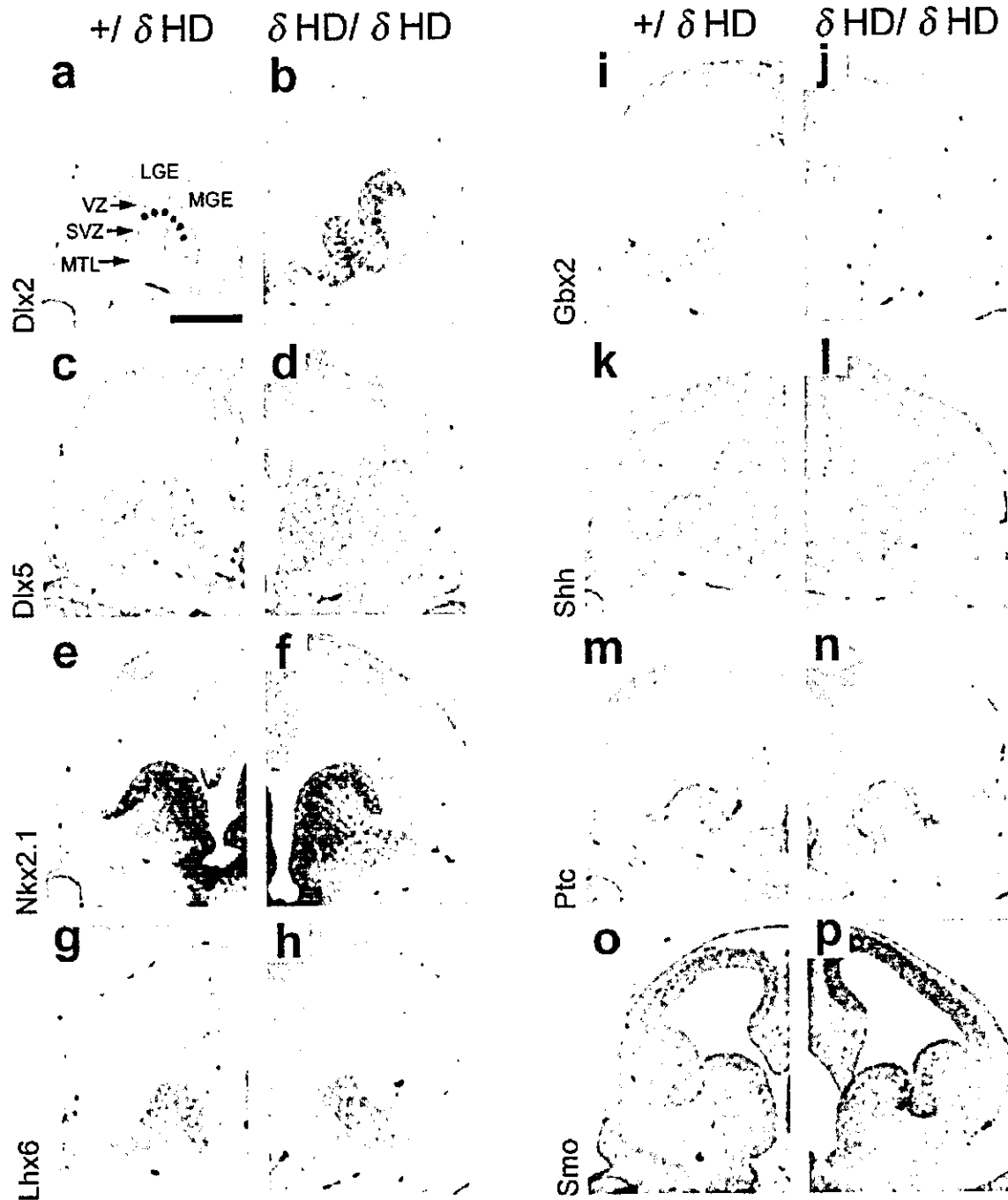
FIG. 3. Molecular marker expression patterns in developing basal forebrain. *In situ* hybridization histochemistry was performed with coronal sections of E12.5 embryos from heterozygous (a, c, e, g, i, k, m and o) and homozygous (b, d, f, h, j, l, n and p) mice. Because the expression patterns are comparable between WT and heterozygous mice, only heterozygous mice are shown in this figure as controls. The markers are indicated at the left of each paired panel: *Dlx2* (a, b), *Dlx5* (c and d), *Nkx2.1* (e and f), *Lhx6* (g and h), *Gbx2* (i and j), *Sonic hedgehog* (k and l), *Patched* (m and n) and *Smoothened* (o and p). Shh, *sonic hedgehog*; Ptc, *patched*; Smo, *smoothened*; VZ, ventricular zone; SVZ, subventricular zone; MTL, mantle layer. The scale bar in (a) represents 500 µm for all panels.

strongly suggesting that neurons expressing GFP in the basal forebrain did not die but transformed to a phenotype other than cholinergic in *L3/Lhx8* δHD/δHD mice. In view of this hypothesis, we next examined distributions of several neurotransmitters, i.e. *enkephalin* (Fig. 6a and b), *neuropeptide Y* (Fig. 6c and d), *somatostatin* (Fig. 6e and f), *substance P* (Fig. 6g and h), galanin (data not shown) and *GAD* (data not shown) of P0 and adult mice (data not shown) in the basal

forebrain. No significant changes of their mRNA expressions were observed.

It has been shown that bone morphogenetic proteins (BMPs), especially *BMP-9*, induce and maintain the cholinergic phenotype in the basal forebrain (Lopez-Coviella *et al.*, 2000). We therefore examined *BMP-9* mRNA expression in the E14.5 basal forebrain of all the genotypes with RT-PCR. BMP-9 mRNA was always detected (Fig. 7).
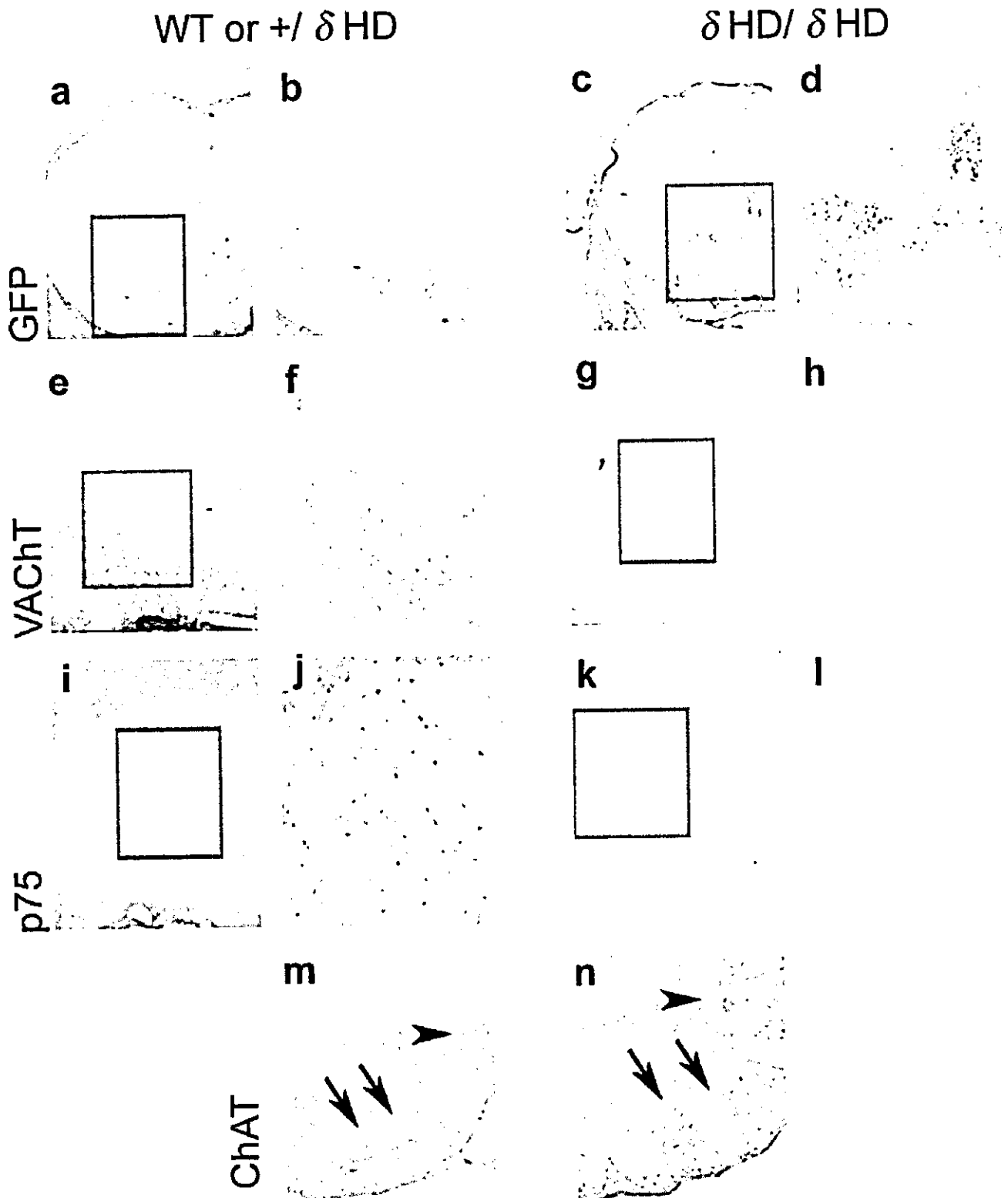
WT or +/ δ HD

δ HD/ δ HD

a   b

c   d

GFP

e   f

g   h

VAChT

i   j

k   l

p75

m

n

ChAT

FIG. 4. Cholinergic neuron marker expressions are not detected in the basal forebrain, but are detected in other regions of the P0 *L3/Lhx8* δHD/δHD mice. Coronal sections of P0 heterozygous (a, b, e and f), WT (i, j and m) and homozygous (c, d, g, h, k, l and n) pups were used for *in situ* hybridization (a–h) or immunohistochemistry (i–n). High-magnification photographs of each boxed area are aligned on the right. *eGFP* mRNA (a–d), *VAChT* mRNA (e–h) and p75 low-affinity NGF receptor (i–l) expression patterns are presented. In the spinal cord of wild-type (m) and δHD/δHD mice (n), ChAT is expressed in the motor neurons (arrows) and in the neurons of the intermediolateral column (arrowhead). The scale bar in (a) represents 1 mm (a and c), 500 μm (b, d, e, g, i, k, m and n), and 200 μm (f, h, j and l).
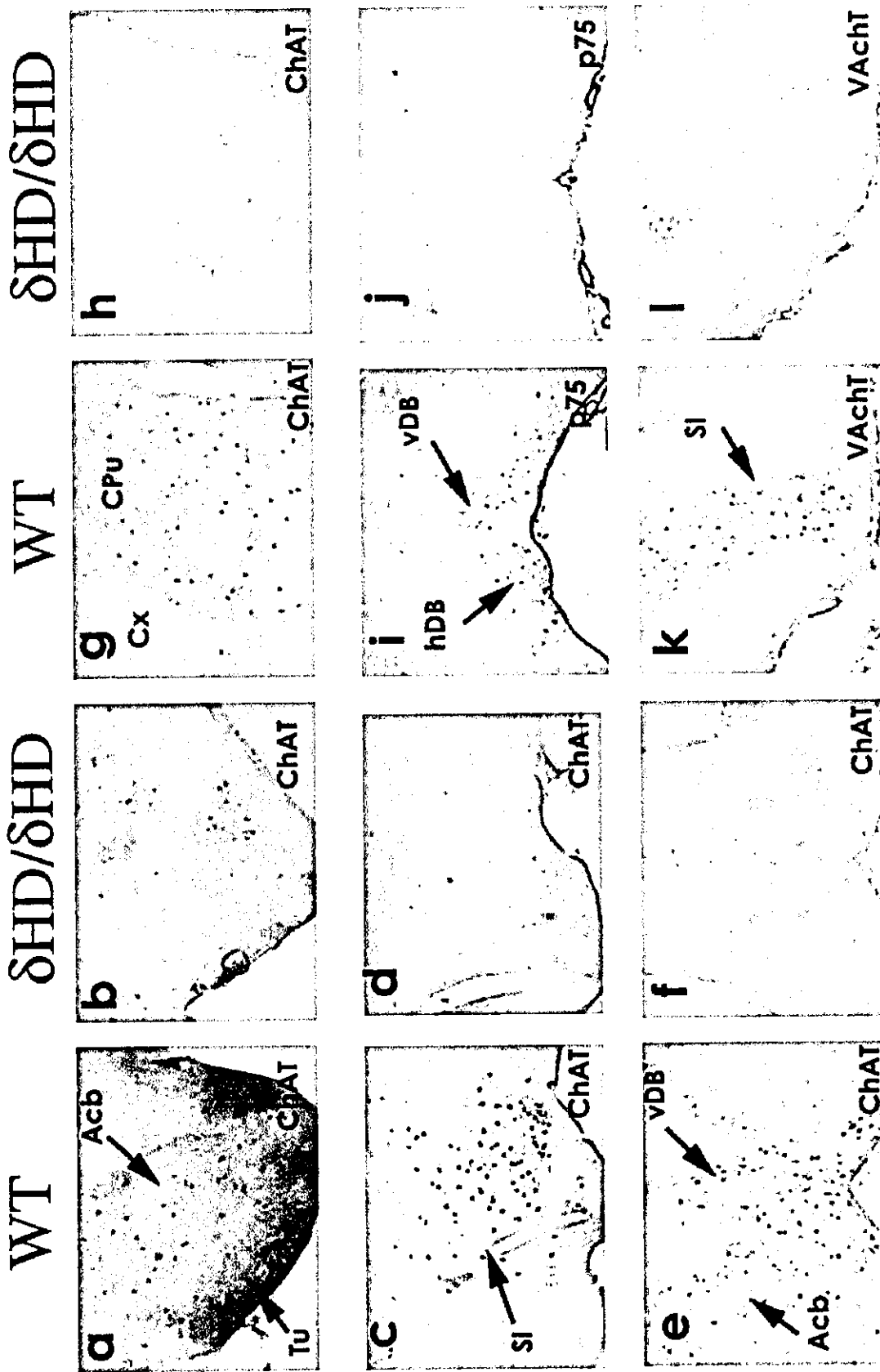
FIG. 5.   The number of ChAT-, p75 low-affinity NGF receptor- or vesicular acetylcholine transporter-positive neurons in the basal forebrain are greatly reduced in adult δHD/δHD mice. Coronal sections of WT (a, c, e, g, i and k) and δHD/δHD (b, d, f, h, j, l) mice were used for immunohistochemistry with an anti-ChAT antibody (a–h), anti-p75 low-affinity NGF receptor (i and j) antibody and anti-VAChT antibody (k and l). Acb, accumbens nucleus; Tu, olfactory tubercle; SI, substantia innominata; vDB, vertical limb of the diagonal band; hDB, horizontal limb of the diagonal band; Cpu, caudate putamen; GP, globus pallidus; CX, cerebral cortex. The scale bar in (b) represents 500 μm for all panels.
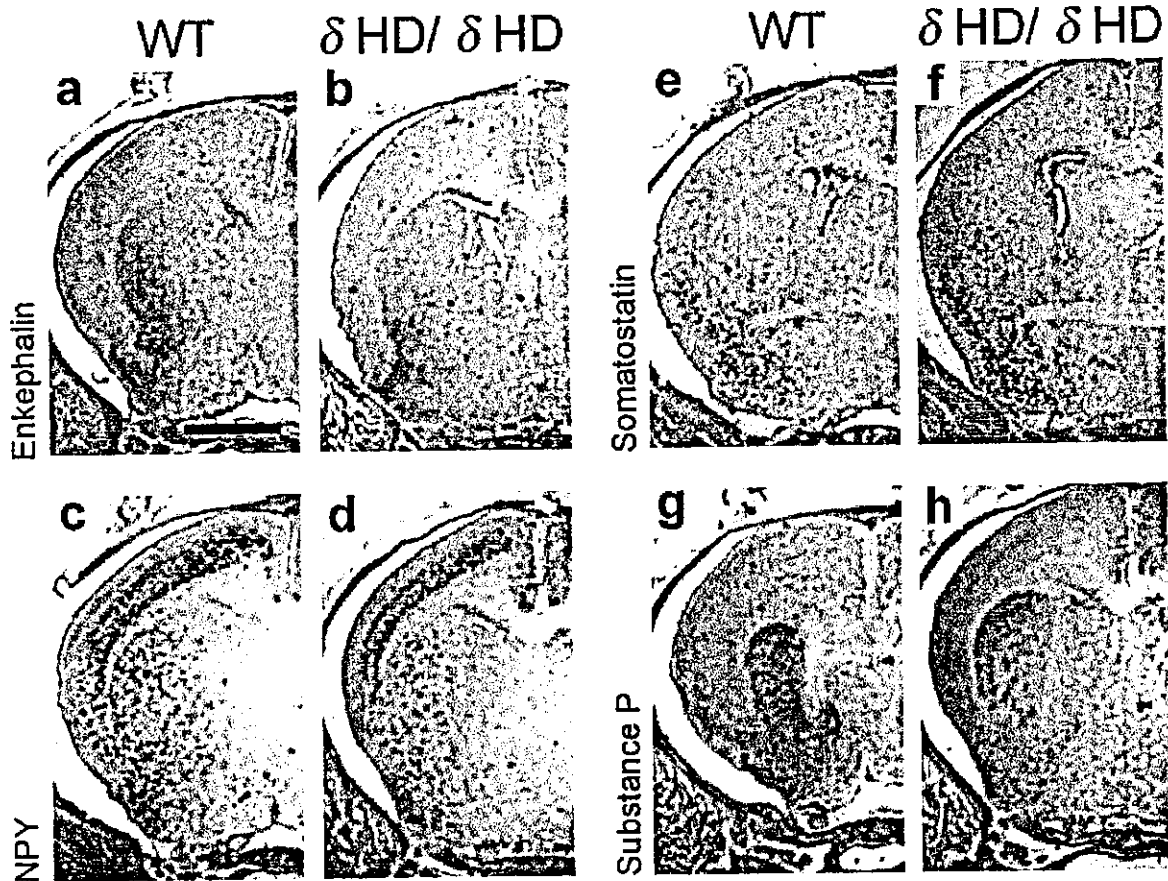
FIG. 6. Almost all neurotransmitter mRNAs distributed in the basal forebrain are expressed normally in the *L3/Lhx8* δHD/δHD mice. Coronal sections of P0 pups from the wild type (WT; a, c, e and g) or P0 homozygous pups (δHD/δHD; b, d, f and h) were hybridized with each probe indicated at the left of each paired panel; enkephalin (a, b), neuropeptide Y (c and d), somatostatin (e and f) and substance P (g and h). NPY, neuropeptide Y. The scale bar represents 1 mm for all panels.

Interneurons in the olfactory bulb, hippocampus and cerebral cortex were normal in L3/Lhx8 δHD/δ HD mice

Most GABAergic interneurons in rodent forebrain are derived from the ventral forebrain; in the olfactory bulb they are derived from the LGE (Anderson *et al.*, 1999); all of them in the hippocampus (Pleasure *et al.*, 2000) and most of them in the neocortex (Anderson *et al.*, 1997) are derived from both the LGE and the MGE.

FIG. 7. *BMP9* mRNA is detected by RT-PCR in *L3/Lhx8* δHD/δHD mice. When we use a cDNA template prepared from the basal forebrain of the E14.5 embryos and mouse genomic DNA (G) as a positive control, we can detect a 90-bp PCR product of *BMP9* in all the genotypes (WT, wild type; +/δ, +/δHD; δ/δ, δHD/δHD). As negative controls we use DNase-treated RNAs as a PCR template. In those cases, only the primer dimers or non-specific PCR products are detected. G, genomic DNA; M, molecular marker.

To test the possibility that interneurons derived from ventral telencephalon could be affected by targeted disruption of *L3/Lhx8*, we compared GABAergic neurons in the olfactory bulb (Fig. 8a and b), hippocampus (Fig. 8c and d) and cerebral cortex (Fig. 8e and f) of P0 mice. We detected GABAergic neurons in each brain region of homozygous mice and their numbers and morphologies were similar to those of WT or heterozygous mice. In addition, Lhx6-expressing cells in the cerebral cortex of homozygous mice also migrate from the MGE, in a manner indistinguishable from WT mice (Fig. 8g and h).
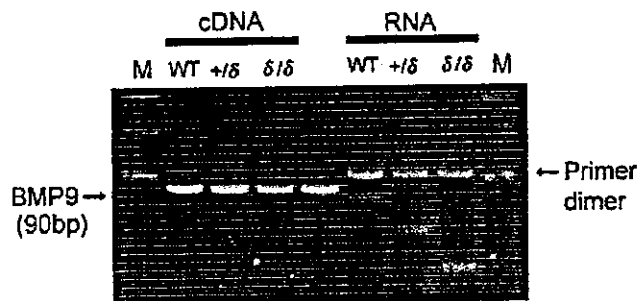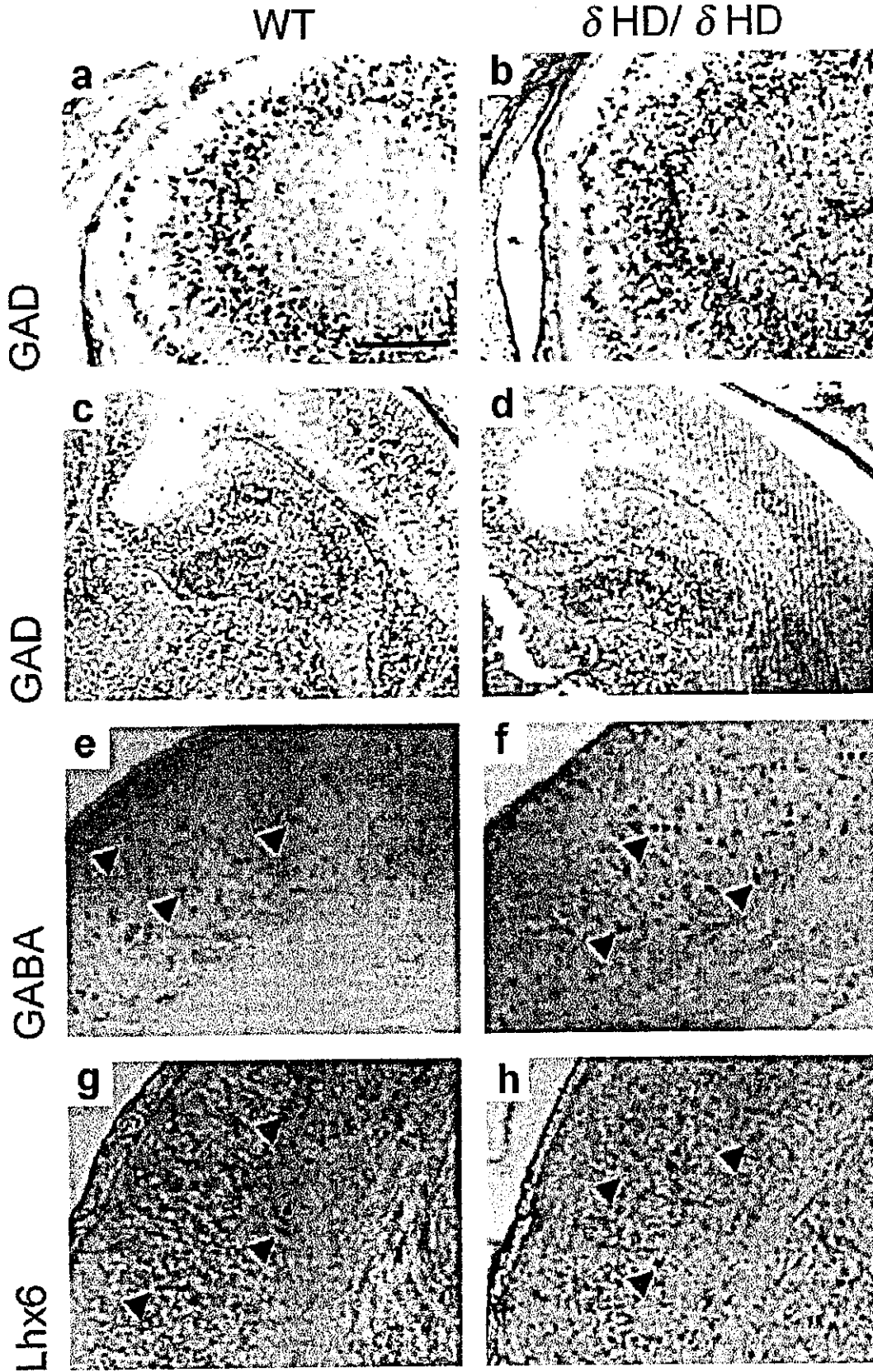
Discussion

Different phenotypes between two lines of L3/Lhx8-targeted mice

Consistent with a previous study (Zhao *et al.*, 1999), *L3/Lhx8* δHD mice also suffered from cleft palates, but the incidence of cleft palate was much higher (about 95% among δHD/δHD mice) than for *L3/Lhx8*−/− mice (60%). The lower incidence of cleft palate in the −/− mice could result from the compensation of the *L3/Lhx8* function by Lhx6, because *L3/Lhx8* and Lhx6 mRNAs were co-expressed in many cells in the MGE and palatal mesenchyme throughout embryonic development (Grigoriou *et al.*, 1998; Zhang *et al.*, 2002). The difference could hardly be attributed to the genetic backgrounds of two lines of *L3/Lhx8*-targeted mice; 129 strain-derived ES cells (R1 used in the previous study of Zhao *et al.*, 1999; D3 used in this study) were

WT δ HD/ δ HD

GAD

GAD

GABA

Lhx6

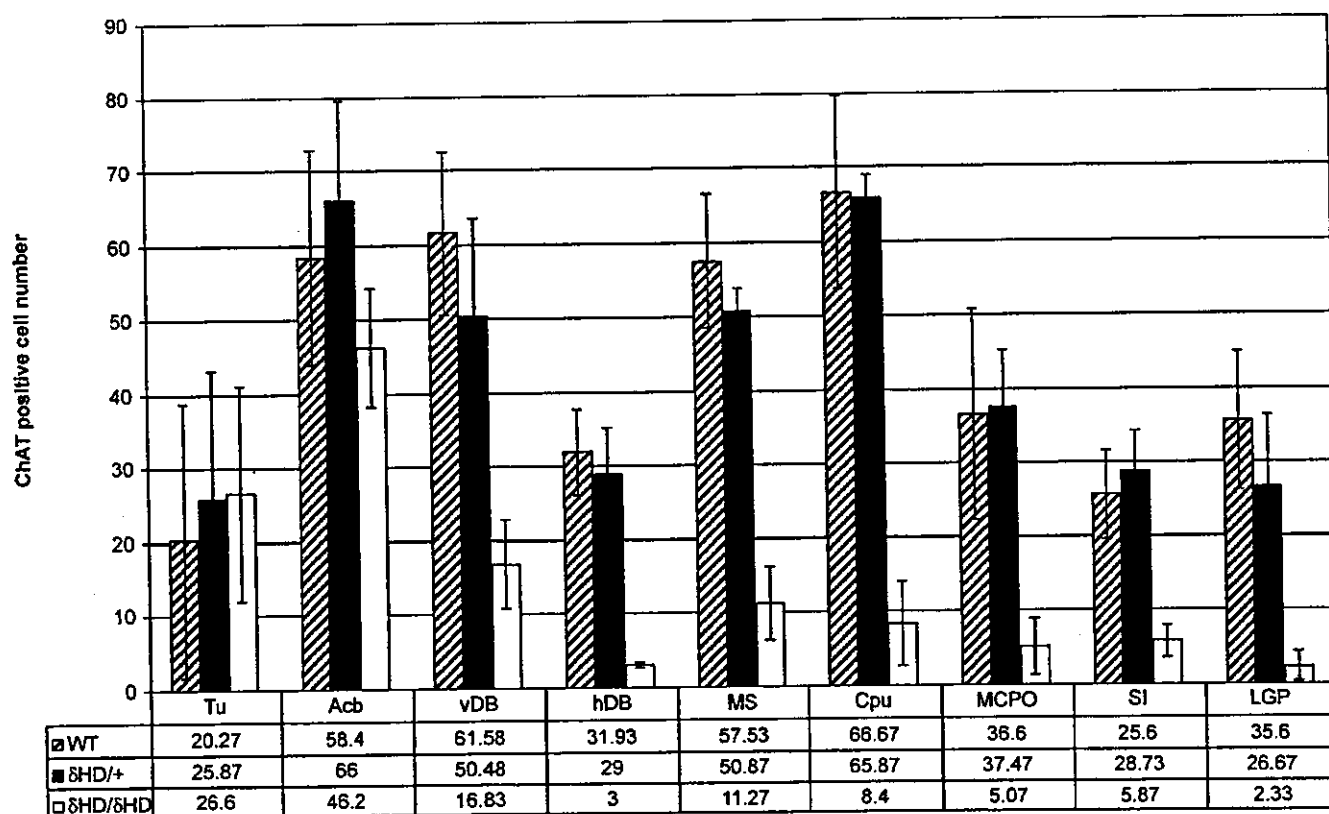|	Tu	Acb	vDB	hDB	MS	Cpu	MCPO	SI	LGP
☑ WT	20.27	58.4	61.58	31.93	57.53	66.67	36.6	25.6	35.6
■ δHD/+	25.87	66	50.48	29	50.87	65.87	37.47	28.73	26.67
☐ δHD/δHD	26.6	46.2	16.83	3	11.27	8.4	5.07	5.87	2.33

Fig. 9. ChAT-immunopositive neurons were counted in each nucleus of adult (1 month old) brain and compared between littermates. We counted immunopositive cells in five sections per one animal, and average numbers of three independent brains are indicated as columns (hatched column, WT; filled column, +/δHD; open column, δHD/δHD) and in Table 1. Error bars indicate the standard deviations. Note that the extent of reduction varies between each nucleus in the δHD/δHD mice as compared with the WT mice. Tu, olfactory tubercle; Acb: accumbens nucleus; vDB, vertical limb of the diagonal band nucleus; hDB, horizontal limb of the diagonal band nucleus; MS, medial septum; Cpu, caudate putamen; MCPO, central subnucleus of the medial preoptic nucleus; SI, substantia innominata; LGP, lateral globus pallidus.

employed and back-crossed with C57BL6 in these lines. Although we do not have direct evidence of a dominant-negative effect exerted by the LIM domain-only protein of L3/Lhx8, it is likely that we could lessen the compensation of Lhx6 with our present strategy. Further studies will be required to elucidate the mechanisms underlying the difference.

Specification of cholinergic neurons in the basal forebrain

Several studies suggest that cholinergic neurons in the basal forebrain are heterogeneous. For example, about 13% of the BFCN co-express galanin (Miller et al., 1998) and some cholinergic neurons co-express Isl-1 whereas others do not (Wang & Liu, 2001). Our study also suggests that L3/Lhx8 plays important roles in the differentiation of some populations of BFCNs, because a great number of the BFCNs were decreased in adult brains of δHD/δHD mice (Fig. 9). While the present study was in preparation, it was reported that L3/Lhx8−/− mice showed reduction of BFCNs, albeit to a lesser extent (25–75% reduction) (Zhao et al., 2003) than that of our mice. The lesser reduction of BFCNs in L3/Lhx8−/− mice might be attributed to the compensation by Lhx6, as in the palate development. The varied

extents of the BFCN reduction between each nucleus of δHD/δHD and −/− mice imply a complex nature to the differentiation of cholinergic neurons. For example, the cholinergic neurons in the olfactory tubercle and accumbens nucleus were spared in both lines of targeted mice. These cholinergic neurons could not be descendants of MGE, but of LGE where neither L3/Lhx8 nor Lhx6 are expressed; or they do not need both L3/Lhx8 and Lhx6 functions. By contrast, cholinergic neurons in the vertical limb of the diagonal band, caudate putamen and globus pallidus require L3/Lhx8 function for their proper differentiation, because even L3/Lhx8−/− mice with possible compensation by Lhx6 lost up to 75% of their cholinergic neurons (Zhao et al., 2003). The fact that eGFP mRNA derived from a recombinant allele of δHD/δHD mice was expressed at P0 in a comparable pattern to that of L3/Lhx8 mRNA in WT mice (Fig. 4a–d) indicates that BFCN precursors do not undergo apoptosis, but adopt a fate other than that of the cholinergic neuron without L3/Lhx8 functions. Neurons positive for enkephalin, neuropeptide Y, somatostatin, substance P, GABA and galanin in the basal forebrain appeared unchanged (Fig. 6), although it would be very difficult to detect a 'slight increase' of certain phenotypes at the expense of the BFCNs, numbers of which are small in the

Fig. 8. GABAergic interneurons in the L3/Lhx8 δHD/δHD mice appear normal. GABAergic interneurons in the olfactory bulb (a and b), hippocampus (c and d) and cerebral cortex (e–h) derived from the basal forebrain are examined. Coronal sections of P0 mice were processed with a GAD probe (a–d), Lhx6 probe (g and h) and anti-GABA antibody (e and f). The scale bar in (a) represents 200 μm (a, b, e, f, g and h) and 500 μm (c and d).

adult brain. Because we failed to detect any significant increase in the number of GAD-positive neurons in the basal forebrain of δHD/δHD mice, we require further study to investoigate this changed fate.

Cholinergic fate is probably determined before birth, because we detected none of the cholinergic markers in the P0 basal forebrain of δHD/δHD mice, whereas we could always observe ChAT-positive BFCNs in P0 WT mice. Consistent with this hypothesis, the expression levels of the two Lhx factors (L3/Lhx8 and Lhx6) are much higher in embryonic than in postnatal brain (Matsumoto et al., 1996; Kimura et al., 1999).

Taking a recent study (Asbreuk et al., 2002) into account, it is likely that sequential and/or simultaneous expressions of the transcription factors, such as L3/Lhx8, Lhx6, Isl-1 and Gbx-1 (and possibly Gbx-2, in this study, Fig. 3i and j), are necessary for proper differentiation of BFCNs. The importance of the combination of multiple transcription factors in neuronal differentiation is reinforced by the following data; migrating cortical interneurons expressing Lhx6, GABA and neuropeptide Y (Marin et al., 2001), which derived from the ventral forebrain (MGE and/or LGE), were detected in δHD/δHD mice and their number did not apparently decrease compared with that in WT mice (Fig. 9). These ventral forebrain-derived cortical interneurons might be descendants of precursor cells expressing Lhx6 (but not L3/Lhx8), which distribute in the relatively posterior part of the MGE. BFCNs could be derived mainly from the anterior part of the MGE (L3/Lhx8 and Lhx6 double-positive precursors).

The present study provides evidence that L3/Lhx8 (and possibly Lhx6) has important roles in the differentiation of BFCNs. This is the first step toward an understanding of how a neuronal precursor adopts a cholinergic fate.

Acknowledgements

Abbreviations

BFCNs, sasal forebrain cholinergic neurons; BMPs, bone morphogenetic proteins; ChAT, choline acetyltransferase; (F)ISH, (fluoresence) in situ hybridization; GFP, green fluorescent protein; LGE, lateral ganglionic eminence; MGE, medial ganglionic eminence; SVZ, subventricular zone; VAChT, VZ, vesicular acetylcholine transporter; ventricular, zone; WT, wild-type.

References

Anderson, S.A., Eisenstat, D.D., Shi, L. & Rubenstein, J.L. (1997) Interneuron migration from basal forebrain to neocortex: dependence on Dlx genes. Science, 278, 474–476.

Anderson, S., Mione, M., Yun, K. & Rubenstein, J.L. (1999) Differential origins of neocortical projection and local circuit neurons: role of Dlx genes in neocortical interneuronogenesis. Cereb. Cortex, 9, 646–654.

Asbreuk, C.H., van Schaick, H.S., Cox, J.J., Kromkamp, M., Smidt, M.P. & Burbach, J.P. (2002) The homeobox genes Lhx7 and Gbx1 are expressed in the basal forebrain cholinergic system. Neuroscience, 109, 287–298.

Bulfone, A., Puelles, L., Porteus, M.H., Frohman, M.A., Martin, G.R. & Rubenstein, J.L. (1993) Spatially restricted expression of Dlx-1, Dlx-2 (Tes-1), Gbx-2, and Wnt- 3 in the embryonic day 12.5 mouse forebrain defines potential transverse and longitudinal segmental boundaries. J. Neurosci., 13, 3155–3172.

Casarosa, S., Fode, C. & Guillemot, F. (1999) Mash1 regulates neurogenesis in the ventral telencephalon. Development, 126, 525–534.

Cheng, L., Chen, C.L., Luo, P., Tan, M., Qiu, M., Johnson, R. & Ma, Q. (2003) Lmx1b, Pet-1, and Nkx2.2 coordinately specify serotonergic neurotransmitter phenotype. J. Neurosci., 23, 9961–9967.

Dawid, I.B., Breen, J.J. & Toyama, R. (1998) LIM domains: multiple roles as adapters and functional modifiers in protein interactions. Trends Genet., 14, 156–162.

Ding, Y.Q., Marklund, U., Yuan, W., Yin, J., Wegman, L., Ericson, J., Deneris, E., Johnson, R.L. & Chen, Z.F. (2003) Lmx1b is essential for the development of serotonergic neurons. Nature Neurosci., 6, 933–938.

Eisenstat, D.D., Liu, J.K., Mione, M., Zhong, W., Yu, G., Anderson, S.A., Ghattas, I., Puelles, L. & Rubenstein, J.L. (1999) DLX-1, DLX-2, and DLX-5 expression define distinct stages of basal forebrain differentiation. J. Comp. Neurol., 414, 217–237.

Ericson, J., Muhr, J., Jessell, T.M. & Edlund, T. (1995) Sonic hedgehog: a common signal for ventral patterning along the rostrocaudal axis of the neural tube. Int. J. Dev. Biol., 39, 809–816.

Everitt, B.J. & Robbins, T.W. (1997) Central cholinergic systems and cognition. Annu. Rev. Psychol., 48, 649–684.

Ferrante, R.J., Beal, M.F., Kowall, N.W., Richardson, E.P. Jr & Martin, J.B. (1987) Sparing of acetylcholinesterase-containing striatal neurons in Huntington's disease. Brain Res., 411, 162–166.

Goridis, C. & Brunet, J.F. (1999) Transcriptional control of neurotransmitter phenotype. Curr. Opin. Neurobiol., 9, 47–53.

Grigoriou, M., Tucker, A.S., Sharpe, P.T. & Pachnis, V. (1998) Expression and regulation of Lhx6 and Lhx7, a novel subfamily of LIM homeodomain encoding genes, suggests a role in mammalian head development. Development, 125, 2063–2074.

Hallonet, M., Hollemann, T., Pieler, T. & Gruss, P. (1999) Vax1, a novel homeobox-containing gene, directs development of the basal forebrain and visual system. Genes Dev., 13, 3106–3114.

Harada, Y.N., Shiomi, N., Koike, M., Ikawa, M., Okabe, M., Hirota, S., Kitamura, Y., Kitagawa, M., Matsunaga, T., Nikaido, O. & Shiomi, T. (1999) Postnatal growth failure, short life span, and early onset of cellular senescence and subsequent immortalization in mice lacking the xeroderma pigmentosum group G gene. Mol. Cell Biol., 19, 2366–2372.

Iseki, K., Hagino, S., Mori, T., Zhang, Y., Yokoya, S., Takaki, H., Tase, C., Murakawa, M. & Wanaka, A. (2002) Increased syndecan expression by pleiotrophin and FGF receptor-expressing astrocytes in injured brain tissue. Glia, 39, 1–9.

Kikuchi, Y., Segawa, H., Tokumoto, M., Tsubokawa, T., Hotta, Y., Uyemura, K. & Okamoto, H. (1997) Ocular and cerebellar defects in zebrafish induced by overexpression of the LIM domains of the islet-3 LIM/homeodomain protein. Neuron, 18, 369–382.

Kimura, S., Hara, Y., Pineau, T., Fernandez-Salguero, P., Fox, C.H., Ward, J.M. & Gonzalez, F.J. (1996) The T/ebp null mouse: thyroid-specific enhancer-binding protein is essential for the organogenesis of the thyroid, lung, ventral forebrain, and pituitary. Genes Dev., 10, 60–69.

Kimura, N., Ueno, M., Nakashima, K. & Taga, T. (1999) A brain region-specific gene product Lhx6.1 interacts with Ldb1 through tandem LIM-domains. J. Biochem. (Tokyo), 126, 180–187.

Kohtz, J.D., Baker, D.P., Corte, G. & Fishell, G. (1998) Regionalization within the mammalian telencephalon is mediated by changes in responsiveness to Sonic Hedgehog. Development, 125, 5079–5089.

Lopez-Coviella, I., Berse, B., Krauss, R., Thies, R.S. & Blusztajn, J.K. (2000) Induction and maintenance of the neuronal cholinergic phenotype in the central nervous system by BMP-9. Science, 289, 313–316.

Marin, O., Baker, J., Puelles, L. & Rubenstein, J.L. (2002) Patterning of the basal telencephalon and hypothalamus is essential for guidance of cortical projections. Development, 129, 761–773.

Marin, O., Yaron, A., Bagri, A., Tessier-Lavigne, M. & Rubenstein, J.L. (2001) Sorting of striatal and cortical interneurons regulated by semaphorin–neuropilin interactions. Science, 293, 872–875.

Matsumoto, K., Tanaka, T., Furuyama, T., Kashihara, Y., Mori, T., Ishii, N., Kitanaka, J., Takemura, M., Tohyama, M. & Wanaka, A. (1996) L3, a novel murine LIM-homeodomain transcription factor expressed in the ventral telencephalon and the mesenchyme surrounding the oral cavity. Neurosci. Lett., 204, 113–116.

Miller, M.A., Kolb, P.E., Planas, B. & Raskind, M.A. (1998) Few cholinergic neurons in the rat basal forebrain coexpress galanin messenger RNA. J. Comp. Neurol., 391, 248–258.

Misawa, H., Nakata, K., Matsuura, J., Nagao, M., Okuda, T. & Haga, T. (2001) Distribution of the high-affinity choline transporter in the central nervous system of the rat. Neuroscience, 105, 87–98.

Nikaido, T., Yokoya, S., Mori, T., Hagino, S., Iseki, K., Zhang, Y., Takeuchi, M., Takaki, H., Kikuchi, S. & Wanaka, A. (2001) Expression of the novel transcription factor OASIS, which belongs to the CREB/ATF family, in mouse embryo with special reference to bone development. *Histochem. Cell Biol.*, **116**, 141–148.

O'Keefe, D.D., Thor, S. & Thomas, J.B. (1998) Function and specificity of LIM domains in *Drosophila* nervous system and wing development. *Development*, **125**, 3915–3923.

Paxinos, G. & Franklin, K.B.J. (2001) *The mouse brain in stereotaxic coordinates.* Academic Press, San Diego, USA.

Pleasure, S.J., Anderson, S., Hevner, R., Bagri, A., Marin, O., Lowenstein, D.H. & Rubenstein, J.L. (2000) Cell migration from the ganglionic eminences is required for the development of hippocampal GABAergic interneurons. *Neuron*, **28**, 727–740.

Saucedo-Cardenas, O., Quintana-Hau, J.D., Le, W.D., Smidt, M.P., Cox, J.J., De Mayo, F., Burbach, J.P. & Conneely, O.M. (1998) Nurr1 is essential for the induction of the dopaminergic phenotype and the survival of ventral mesencephalic late dopaminergic precursor neurons. *Proc. Natl Acad. Sci. USA*, **95**, 4013–4018.

Segawa, H., Miyashita, T., Hirate, Y., Higashijima, S., Chino, N., Uyemura, K., Kikuchi, Y. & Okamoto, H. (2001) Functional repression of Islet-2 by disruption of complex with Ldb impairs peripheral axonal outgrowth in embryonic zebrafish. *Neuron*, **30**, 423–436.

Sussel, L., Marin, O., Kimura, S. & Rubenstein, J.L. (1999) Loss of Nkx2.1 homeobox gene function results in a ventral to dorsal molecular respecification within the basal telencephalon: evidence for a transformation of the pallidum into the striatum. *Development*, **126**, 3359–3370.

Taira, M., Otani, H., Saint-Jeannet, J.P. & Dawid, I.B. (1994) Role of the LIM class homeodomain protein Xlim-1 in neural and muscle induction by the Spemann organizer in *Xenopus*. *Nature*, **372**, 677–679.

Tojo, M., Mori, T., Kiyosawa, H., Honma, Y., Tanno, Y., Kanazawa, K.Y., Yokoya, S., Kaneko, F. & Wanaka, A. (1999) Expression of sonic hedgehog signal transducers, patched and smoothened, in human basal cell carcinoma. *Pathol. Int.*, **49**, 687–694.

Toresson, H., Potter, S.S. & Campbell, K. (2000) Genetic control of dorsal–ventral identity in the telencephalon: opposing roles for Pax6 and Gsh2. *Development*, **127**, 4361–4371.

Wang, H.F. & Liu, F.C. (2001) Developmental restriction of the LIM homeodomain transcription factor Islet-1 expression to cholinergic neurons in the rat striatum. *Neuroscience*, **103**, 999–1016.

Whitehouse, P.J., Price, D.L., Struble, R.G., Clark, A.W., Coyle, J.T. & Delon, M.R. (1982) Alzheimer's disease and senile dementia: loss of neurons in the basal forebrain. *Science*, **215**, 1237–1239.

Yun, K., Potter, S. & Rubenstein, J.L. (2001) Gsh2 and Pax6 play complementary roles in dorsoventral patterning of the mammalian telencephalon. *Development*, **128**, 193–205.

Zetterstrom, R.H., Solomin, L., Jansson, L., Hoffer, B.J., Olson, L. & Perlmann, T. (1997) Dopamine neuron agenesis in Nurr1-deficient mice. *Science*, **276**, 248–250.

Zhang, Y., Mori, T., Takaki, H., Takeuch, M., Iseki, K., Hagino, S., Murakawa, M., Yokoya, S. & Wanaka, A. (2002) Comparison of the expression patterns of two LIM-homeodomain genes, Lhx6 and L3/Lhx8, in the developing palate. *Orthod. Craniofac. Res.*, **5**, 65–70.

Zhao, Y., Guo, Y.J., Tomac, A.C., Taylor, N.R., Grinberg, A., Lee, E.J., Huang, S. & Westphal, H. (1999) Isolated cleft palate in mice with a targeted mutation of the LIM homeobox gene lhx8. *Proc. Natl. Acad. Sci. USA*, **96**, 15002–15006.

Zhao, Y., Marin, O., Hermesz, E., Powell, A., Flames, N., Palkovits, M., Rubenstein, J.L. & Westphal, H. (2003) The LIM-homeobox gene Lhx8 is required for the development of many cholinergic neurons in the mouse forebrain. *Proc. Natl Acad. Sci. USA*, **100**, 9005–9010.

Short Communication

Ultrastructural Localization of High-Affinity Choline Transporter in the Rat Neuromuscular Junction: Enrichment on Synaptic Vesicles

KAZUKO NAKATA,[1] TAKASHI OKUDA,[2] AND HIDEMI MISAWA[1]*
[1]*Department of Neurology, Tokyo Metropolitan Institute for Neuroscience, Tokyo 183-8526, Japan*
[2]*Department of Neurochemistry, Faculty of Medicine, University of Tokyo, Tokyo 113-0033, Japan*

ABSTRACT   In cholinergic neurons, Na^+- and Cl^--dependent, hemicholinium-3-sensitive, high-affinity choline uptake system is thought to be the rate-limiting step in acetylcholine (ACh) synthesis. The system is highly regulated by neuronal activity; the choline uptake is increased by a condition in which ACh release is favored. Here we analyzed the ultrastructural localization of the high-affinity choline transporter (CHT) in the rat neuromuscular junctions with two separate antibodies. The majority (>90%) of immunogold labeling of CHT was observed on synaptic vesicles rather than the presynaptic plasma membrane. Less than 5% of the gold-silver particles were associated with the plasma membrane, and more than 70% of such particles were localized within or in close vicinity to presynaptic active zones. Our morphological data support the recent hypothesis that trafficking of CHT from synaptic vesicles to the plasma membrane couples neuronal activity and choline uptake. **Synapse 53:53–56, 2004.**

Acetylcholine (ACh) is a major neurotransmitter both in the central and peripheral nervous system. ACh is synthesized from choline and acetyl-CoA by the enzyme choline acetyltransferase (ChAT), which is specifically expressed in cholinergic neurons. For efficient and sustained neurotransmission, cholinergic neurons are endowed with a unique high-affinity choline uptake (HACU) system (Haga, 1971; Haga and Noda, 1973; Kuhar et al., 1973; Kuhar and Murrin, 1978; Tucek, 1985; Yamamura and Snyder, 1972). The HACU activity is Na^+- and Cl^--dependent and inhibited by hemicholinium-3 (HC-3) (Kuhar and Zarbin, 1978; Yamamura and Snyder, 1972, 1973). Studies using brain synaptosomes and slices demonstrated that the HACU system is the rate-limiting step in ACh synthesis, and the HACU activity is highly regulated by neuronal activity (Murrin et al., 1977; Saltarelli et al., 1987; Simon and Kuhar, 1975). Owing to a lack of structural information, the cellular mechanism governing the activity-dependent regulation of the HACU activity remains largely unknown.

By using information from the *Caenorhabditis elegans* Genome Project and expression screening in *Xe-* *nopus laevis* oocytes, Okuda et al. (2000) first cloned the nematode high-affinity choline transporter (cho-1). Later, mammalian cDNA clones encoding the high-affinity choline transporter (CHT) were isolated and characterized from rat (Okuda et al., 2000), human (Apparsundaram et al., 2000; Okuda and Haga, 2000), and mouse (Apparsundaram et al., 2001). Light microscopic immunohistochemical studies in rodents (Ferguson et al., 2003; Lips et al., 2002; Misawa et al., 2001) and primates (Kobayashi et al., 2002; Kus et al., 2003; Misawa et al., 2001) showed that CHT was uniquely expressed in all major cholinergic cell groups and enriched in their projection fields, being consistent with the known function of CHT at cholinergic axon terminals. Recently, Ferguson et al. (2003) showed, by using

Fig. 1. Immunoelectron photomicrographs of neuromuscular junctions in the rat diaphragms labeled with anti-CHT antibody against GST-fusion protein (a, b) or with anti-CHT antibody against C-terminal peptide (c, d). The silver-enhanced gold particles are mostly associated with synaptic vesicles, and occasionally with the plasma membrane (arrows) in the phrenic motor axon terminals (T) forming typical neuromuscular junctions with the diaphragm muscle (M). Some endosome-like irregular vesicles (arrowheads in d) are associated with the immuno-particles. Scale bars = 500 nm in a, c (low-magnification images); 100 nm in b, d (high-magnification images, different section from a and c).

immunoelectron microscopy and biochemical characterization, that CHT was enriched on small presynaptic vesicles in the cholinergic terminals in the rat facial motor nucleus and striatum. In the present study, we analyzed the ultrastructural localization of CHT in rat neuromuscular junctions (NMJ) with two separate antibodies against CHT.

All the procedures conducted in this study were approved by the Institutional Animal Care and Use Committee at Tokyo Metropolitan Institute for Neuroscience. Six adult female Sprague Dawley rats (250–300 g; SLC, Shizuoka, Japan) were used. Animals were deeply anesthetized with sodium pentobarbital (150 mg/kg) and perfused through the aortic cone at a flow rate of 20 ml/min with 50 ml of 0.1 M phosphate buffer pH 7.4 containing 0.9% NaCl (PBS), followed by 250 ml of 4% paraformaldehyde in 0.1 M phosphate buffer (PB, pH 7.4) containing 0.1% glutaraldehyde and 0.2% saturated picric acid. Whole diaphragms were removed and postfixed in the same fixative for 2 h at 4°C. After fixation, the diaphragms were cut into 1.5–2-mm-square pieces and blocked in 3% normal goat serum (NGS; Vector Labs, Burlingame, CA) in 0.02 M PBS containing 0.01% saponin (PBS-S) overnight at 4°C. The diaphragm pieces were then incubated for 3 days

at 4°C with 80 ng/ml of affinity-purified anti-CHT rabbit IgG against the rat CHT C-terminal region (amino acids 502–580) fused to glutathione S-transferase (GST) (Misawa et al., 2001) or with 25 ng/ml of affinity-purified anti-CHT rabbit IgG against the CHT peptide (C-terminal 15 amino acids; Kobayashi et al., 2002) in 3% NGS in PBS-S. After several washes in PBS-S, the pieces were incubated in a 1:100 dilution of affinity-purified goat anti-rabbit Fab' fragments conjugated to 1.4-nm colloidal gold particles (NANOGOLD-Fab' conjugates; Nanoprobes, Yaphank, NY) in 3% NGS in PBS-S for 16 h at 4°C. The pieces were rinsed in PBS, postfixed for 15 min in 1% glutaraldehyde in PBS, and rinsed in distilled water. The conjugated gold particles were silver-enhanced in the dark with HQ Silver Enhancement Kit (Nanoprobes) for 2 min at room temperature. The labeled sections were fixed in 1% osmium tetroxide for 30 min at 4°C, dehydrated through a graded series of ethanol solutions and finally propylene oxide, and embedded in Quetol 812 (Nissin EM, Tokyo, Japan). Once the resin had polymerized, approximately 3-μm sections were cut and examined with a light microscope and the regions containing NMJ were selected for electron microscopy. The sections were re-embedded in Quetol 812, and then cut into ultrathin

sections on an ultramicrotome (MT6000; RMC Inc., Tucson, AZ). The ultrathin sections were counter-stained with Reynold's lead citrate and uranyl acetate and examined with an electron microscope (H7500; Hitachi, Tokyo, Japan) at 20,000× magnification. To quantify immunogold labeling in subcellular compart-ments in the motor nerve terminal, electron micro-scopic images were printed out and silver-gold particles were counted. A total of 12 presynaptic terminals with good morphological preservation were analyzed.

The two polyclonal antibodies specific to CHT used in this study exhibited almost the same pattern of CHT localization in the motor nerve terminals (Fig. 1). Sur-prisingly, the majority of CHT immunogold-silver par-ticles were located on synaptic vesicles; only a small portion of CHT immunoreactivity was associated with the plasma membrane. The synaptic vesicles in motor axon terminals labeled with the silver grains had usu-ally spherical and occasionally endosome-like irregular morphology (Fig. 1d). We counted a total of 1,139 sil-ver-enhanced gold particles and categorized them as either synaptic vesicle-associated, plasma membrane-associated, or others (associated with mitochondria, cytoplasm, or unidentified compartments) (Fig. 2a). The plasma membrane-associated particles were counted when the immuno-particles were located within 50 nm from the plasma membrane. Among the plasma membrane-associated CHT immuno-particles (48 particles), a large portion (>70%) was located within or in close vicinity (within 100 nm) to the active zones, where the nerve terminal directly opposes junc-tional folds in the postsynaptic membrane (Figs. 1, 2b). We categorized 41% of the linear distance of the pre-synaptic membrane (16.4 μm) as "active zones" out of the total length of the presynaptic membrane analyzed (40 μm).

We report here the first description of the immuno-electron microscopic localization of CHT in the rat NMJ, the best characterized of all cholinergic synapses (Hall and Sanes, 1993; Sanes and Lichtman, 1999). Two kinds of polyclonal antibody against CHT gave the same pattern of labeling in NMJ; >90% on the synaptic vesicles and <5% on the plasma membranes. Further-more, the stereotypic well-characterized structure of the NMJ enabled us to quantify a fine localization of CHT in the presynaptic plasma membrane; CHT im-muno-particles were preferentially found at the pre-synaptic active zones or its vicinity. The active zones are sites where synaptic vesicles fuse to the plasma membrane and release their content (ACh) to the syn-aptic cleft. The preferential localization of CHT at the active zones possibly suggests that CHT is delivered to the plasma membrane from synaptic vesicles via mem-brane fusion. Recently, Ferguson et al. (2003) reported, by using immunoelectron microscopy, that a large por-tion of CHT immunoreactivity was localized on synap-tic vesicles in cholinergic presynaptic terminals in the
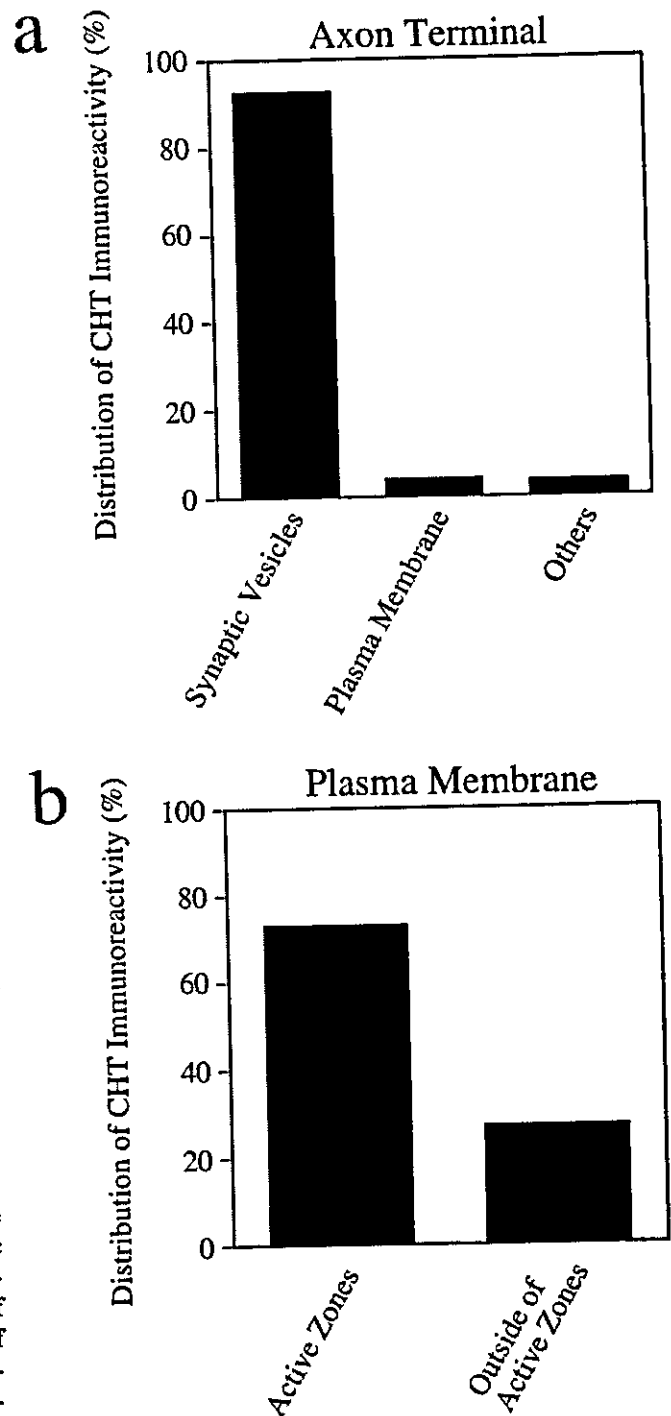

Fig. 2. Quantitative analysis of the subcellular distribution of CHT immunoreactivity in the phrenic motor axon terminals (a) and within the plasma membrane (b). Percentage of immunogold particles is calculated by dividing the number associated with each compart-ment by the total number of particles counted (a, 1,139; b, 48). We counted 736 particles in 7 terminals stained with anti-CHT antibody against GST-fusion protein (30 particles were on the plasma mem-brane), and 403 particles in 5 terminals stained with anti-CHT anti-body against C-terminal peptide (18 particles on the plasma mem-brane).

facial motor nucleus and striatum. Moreover, by using biochemical characterization, they presented a novel and intriguing hypothesis that neuronal activity triggers CHT trafficking from synaptic vesicles to the plasma membrane where levels of choline-uptake couples to ACh release. Although we cannot rule out the possibility that CHT functions as a vesicular transporter for choline or as yet unidentified substrates on synaptic vesicles, the immunoelectron microscopic data presented here strongly support Ferguson et al.'s (2003) hypothesis.

Our immunoelectron microscopic analysis demonstrates that only a small portion (<5%) of CHT immunoreactivity is associated with the plasma membrane. This low percentage possibly suggests that CHT undergoes efficient recovery from the plasma membrane to intracellular vesicles by an endocytic pathway. Furthermore, we occasionally observed CHT immuno-particles on pleiomorphic vesicles, possible endocytic organelles (Fig. 1d). In accordance with this observation, recent CHT transfection analyses in cultured cells demonstrate that CHT is efficiently and constitutively internalized by a clathrin-mediated endocytic pathway (Ferguson and Blakely, 2004; Ribeiro et al., 2003).

In aging and in Alzheimer's disease, dysfuction of cholinergic neurons is well correlated with a decline in cognitive function, and acetylcholinesterase (AChE) inhibitors are so far the only class of drugs for treatment of these disorders. The activity-dependent trafficking model will provide a basis for CHT as a potential new therapeutic target for these disorders.

ACKNOWLEDGMENTS

REFERENCES

Apparsundaram S, Ferguson SM, George Jr AL, Blakely RD. 2000. Molecular cloning of a human, hemicholinium-3-sensitive choline transporter. Biochem Biophys Res Commun 276:862–867.

Apparsundaram S, Ferguson SM, Blakely RD. 2001. Molecular cloning and characterization of a murine hemicholinium-3-sensitive choline transporter. Biochem Soc Trans 29:711–716.

Ferguson SM, Blakely RD. 2004. The choline transporter resurfaces: new roles for synaptic vesicles? Mol Interv 4:22–37.

Ferguson SM, Savchenko V, Apparsundaram S, Zwick M, Wright J, Heilman CJ, Yi H, Levey AI, Blakely RD. 2003. Vesicular localization and activity-dependent trafficking of presynaptic choline transporters. J Neurosci 23:9697–9709.

Haga T. 1971. Synthesis and release of [^{14}C]acetylcholine in synaptosomes. J Neurochem 18:781–798.

Haga T, Noda H. 1973. Choline uptake system of rat brain synaptosomes. Biochim Biophys Acta 291:564–575.

Hall ZW, Sanes JR. 1993. Synaptic structure and development: the neuromuscular junction. Cell 72:99–121.

Kobayashi Y, Okuda T, Fujioka Y, Matsumura G, Nishimura Y, Haga T. 2002. Distribution of the high-affinity choline transporter in the human and macaque monkey spinal cord. Neurosci Lett 317:25–28.

Kuhar MJ, Murrin LC. 1978. Sodium-dependent, high-affinity choline uptake. J Neurochem 30:15–21.

Kuhar MJ, Zarbin MA. 1978. Synaptosomal transport: a chloride dependence for choline, GABA, glycine and several other compounds. J Neurochem 31:251–256.

Kuhar MJ, Sethy VH, Roth RH, Aghajanian GK. 1973. Choline: selective accumulation by central cholinergic neurons. J Neurochem 20:581–593.

Kus L, Borys E, Chu YP, Ferguson SM, Blakely RD, Emborg ME, Kordower JH, Levey AI, Mufson EJ. 2003. Distribution of high affinity choline transporter immunoreactivity in the primate central nervous system. J Comp Neurol 463:341–357.

Lips KS, Pfeil U, Haberberger RV, Kummer W. 2002. Localization of the high-affinity choline transporter-1 in the rat skeletal motor unit. Cell Tissue Res 307:275–280.

Misawa H, Nakata K, Matsuura J, Nagao M, Okuda T, Haga T. 2001. Distribution of the high-affinity choline transporter in the central nervous system of the rat. Neuroscience 105:87–98.

Murrin LC, DeHaven RN, Kuhar MJ. 1977. On the relationship between [^{3}H]choline uptake activation and [^{3}H]acetylcholine release. J Neurochem 29:681–687.

Okuda T, Haga T. 2000. Functional characterization of the human high-affinity choline transporter. FEBS Lett 484:92–97.

Okuda T, Haga T, Kanai Y, Endou H, Ishihara T, Katsura I. 2000. Identification and characterization of the high-affinity choline transporter. Nature Neurosci 3:120–125.

Ribeiro FM, Alves-Silva J, Volknandt W, Martins-Silva C, Mahmud H, Wilhelm A, Gomez MV, Rylett RJ, Ferguson SS, Prado VF, Prado MA. 2003. The hemicholinium-3 sensitive high affinity choline transporter is internalized by clathrin-mediated endocytosis and is present in endosomes and synaptic vesicles. J Neurochem 87:136–146.

Saltarelli MD, Lowenstein PR, Coyle JT. 1987. Rapid in vivo modulation of [^{3}H]hemicholinium-3 binding sites in rat striatal slices. Eur J Pharmacol 135:35–40.

Sanes JR, Lichtman JW. 1999. Development of the vertebrate neuromuscular junction. Annu Rev Neurosci 22:389–442.

Simon JR, Kuhar MG. 1975. Impulse-flow regulation of high affinity choline uptake in brain cholinergic nerve terminals. Nature 255:162–163.

Tucek S. 1985. Regulation of acetylcholine synthesis in the brain. J Neurochem 44:11–24.

Yamamura HI, Snyder SH. 1972. Choline: high-affinity uptake by rat brain synaptosomes. Science 178:626–628.

Yamamura HI, Snyder SH. 1973. High affinity transport of choline into synaptosomes of rat brain. J Neurochem 21:1355–1374.

Synthesis, localization and externalization of galectin-1 in mature dorsal root ganglion neurons and Schwann cells

Kazunori Sango,[1] Akiko Tokashiki,[1] Kyoko Ajiki,[1] Masao Horie,[1] Hitoshi Kawano,[1] Kazuhiko Watabe,[2] Hidenori Horie[3,4] and Toshihiko Kadoya[5]

[1]Department of Developmental Morphology, Tokyo Metropolitan Institute for Neuroscience, 2–6 Musashidai, Fuchu-shi, Tokyo 183–8526, Japan

[2]Department of Molecular Neuropathology, Tokyo Metropolitan Institute for Neuroscience, Fuchu-shi, Tokyo 183–8526, Japan

[3]Advanced Research Center for Biological Science, Waseda University, 2-7-5 Higashifushimi, Nishitokyo-shi, Tokyo 202–0021, Japan

[4]Brain Information Science Institute, Corporate Research Center, Fuji Xerox, 430 Sakai, Nakai-machi, Ashigarakami-gun, Kanagawa 259–0157, Japan

[5]R&D Center, Production Department, Pharmaceutical Division, Kirin Brewery Co. Ltd, Takasaki, Gunma 370–0013, Japan

Abstract

We recently confirmed that oxidized galectin-1 is a novel factor enhancing axonal growth in peripheral nerves after axotomy, but the process of extracellular release and oxidization of endogenous galectin-1 in the injured nervous tissue remains unknown. In the present study, we examined the distribution of galectin-1 in adult rat dorsal root ganglia (DRG) *in vivo* and *in vitro*. By RT-PCR analysis and *in situ* hybridization histochemistry, galectin-1 mRNA was detected in both DRG neurons and non-neuronal cells. Immunohistochemical analyses revealed that galectin-1 was distributed diffusely throughout the cytoplasm in smaller diameter neurons and Schwann cells in DRG sections. In contrast, the immunoreactivity for galectin-1 was detected in almost all DRG neurons from an early stage in culture (3 h after seeding) and was restricted to the surface and/or extracellular region of neurons and Schwann cells at later stages in culture. In a manner similar to the primary cultured cells, we also observed the surface and extracellular expression of this molecule in immortalized adult mouse Schwann cells (IMS32). Western blot analysis has revealed that both reduced and oxidized forms of galectin-1 were detected in culture media of DRG neurons and IMS32. These findings suggest that galectin-1 is externalized from DRG neurons and Schwann cells upon axonal injury. Some of the molecules in the extracellular milieu may be converted to the oxidized form, which lacks lectin activity but could act on neural tissue as a cytokine.

Introduction

Galectin-1 is a member of the galectins, a family of β-galactoside-binding animal lectin (Barondes *et al.*, 1994; Cooper & Barondes, 1999). It is a homodimer with a subunit molecular weight of 14.5 kDa and exhibits lectin activity only in the reduced form (de Waard *et al.*, 1976; Kasai & Hirabayashi, 1996; Perillo *et al.*, 1998). It has been suggested that this lectin plays roles in a wide variety of biological functions such as cell growth and differentiation, apoptosis, cell adhesion, tumour spreading, neurite outgrowth and inflammatory response (Outenreath & Jones, 1992; Mahanthappa *et al.*, 1994; Perillo *et al.*, 1995, 1998; Puche *et al.*, 1996; Rabinovich *et al.*, 2000a,b, 2002). Despite lacking a signal leading peptide, galectin-1 has been reported as being externalized from myogenic cells (Cooper & Barondes, 1990), neuroblastoma cells (Avellana-Adalid *et al.*, 1994), Chinese hamster ovary (CHO) cells (Cho & Cummings, 1995) and human leukaemia cell lines (Lutomski *et al.*, 1997). These findings suggested a pathway for the extracellular release of galectin-1 which is distinct from the classic secretory pathway (Cooper & Barondes, 1990; Cleves *et al.*, 1996; Hughes, 1999). Some other members of galectin

family, namely galectin-3 (Mehul & Hughes, 1997) and galectin-4 (Danielsen & van Deurs, 1997), are subject to externalization in a manner similar to galectin-1. It has been suggested that, following externalization, some of the galectin molecules associate with surface or extracellular matrix glycoconjugates where lectin activity is stabilized while the others, free from glycoconjugate ligands, are rapidly oxidized and inactivated in the nonreducing extracellular environment (Tracey *et al.*, 1992; Cho & Cummings, 1995). In contrast to the concept that galectin-1 is biologically active only in the reduced form, we introduced oxidized galectin-1 as a novel factor enhancing axonal regeneration in peripheral nerves (Horie *et al.*, 1999; Inagaki *et al.*, 2000; Fukaya *et al.*, 2003). Oxidized galectin-1 lacked lectin activity, but it exhibited marked axonal regeneration-promoting activity at concentrations (pg/mL range) substantially lower than those at which the lectin effects of galectin-1 were exhibited in neuronal cells *in vitro* (> ng/mL) (Outenreath & Jones, 1992; Puche *et al.*, 1996). Taking these findings into consideration, oxidized galectin-1 is likely to act on nervous tissue not as a lectin but as a cytokine.

Galectin-1 is expressed in dorsal root ganglion (DRG) neurons and motor neurons with immunoreactivity localized to neuronal cell bodies, axons and Schwann cells of adult rodents (Regan *et al.*, 1986; Hynes *et al.*, 1990; Fukaya *et al.*, 2003). After axonal injury, cytosolic reduced galectin-1 is likely to be externalized from growing

axons and reactive Schwann cells to an extracellular space, where some of the molecule may be converted to the oxidized form and enhance axonal regeneration (Horie & Kadoya, 2000). However, extracellular release of galectin-1 from mature neurons and/or non-neuronal cells after axotomy remains to be clarified. In the present study, we examined histochemical localization of galectin-1 in adult rat DRG both *in vivo* and *in vitro*.

Materials and methods

Animals

Three-month-old female Sprague-Dawley rats were used. All experiments were conducted in accordance with the Guideline for the Care and Use of Animals (Tokyo Metropolitan Institute for Neuroscience, 2000).

RT-PCR analysis

The rats were anaesthetized with ether and killed. Thirty-five DRG (from the cervical to sacral levels) with associated nerve bundles and kidneys were dissected and removed from each animal. Nerve bundles were severed from ganglia, using a sharp blade. Each tissue (ganglia, spinal nerve fibres or kidneys) was separately collected in a sterile tube and stored at $-80\,°C$. Total RNA was isolated from these tissues using Trizol reagent (Invitrogen, Groningen, Netherlands), and was reverse transcribed with M-MLV reverse transcriptase (Invitrogen) and pd(N)$_6$ random primer (Amersham Biosciences Corp., Piscataway, NJ, USA) (Sango *et al.*, 2002b). The synthesized cDNA was used as a template for the PCR reaction. The PCR primers were designed to amplify the 408 bp of rat galectin-1 open reading frame; sense primer, 5'-ATGGCCTGTGGTCTGGTCGCC-3' and antisense primer, 5'-TCAC-TCAAAGGCCACACACTT-3' (GenBank Accession No. M19036) (Clerch *et al.*, 1988). PCR was performed in a 25-μL mixture solution containing 0.2 mM dNTP mix, 10× PCR buffer with 25 mM MgCl$_2$, 0.5 μM of each primer and 0.625 U of AmpliTaq Gold DNA polymerase (Applied Biosystems, Foster City, CA, USA). After denaturation at $95\,°C$ for 9 min, the PCR reaction was cycled 30 times at $95\,°C$ for 1 min, $55\,°C$ for 1 min and $72\,°C$ for 2 min. The PCR products were separated by electrophoresis through 2% agarose gel and visualized with ethidium bromide staining.

Preparation of the plasmid containing rat galectin-1 cDNA

The plasmid containing the rat galectin-1 cDNA fragment was created by PCR cloning as described previously (Toba *et al.*, 2002). Briefly, the 408-bp fragment amplified by PCR was subcloned into pGEM-T Easy Vector (Promega Corp., Madison, WI, USA) according to the manufacturer's instructions, and the resulting plasmid DNA was sequenced (Sawady Custom Technology Service, Tokyo, Japan).

In situ hybridization

We examined mRNA expression patterns of galectin-1 by *in situ* hybridization histochemistry as described previously (Ichikawa *et al.*, 1997) with slight modifications. Digoxigenin-labelled antisense and sense cRNA probes for galectin-1 were prepared using DIG RNA labelling mix (Roche Diagnostics, GmbH, Mannheim, Germany) with linearized plasmid DNA according to the manufacturer's instructions. The rats were anaesthetized by intraperitoneal injection of pentobarbital sodium (50 mg/kg), and then briefly perfused through the left cardiac ventricle with 100 mM phosphate-buffered saline (PBS, pH 7.4) followed by 4% paraformaldehyde. Lumbar DRG dissected from the rats were processed for paraffin embedding and sectioned into 5-μm-thick slices. Deparaffinized sections were treated with 0.2 N HCl for 15 min, 0.2% triton-X for 10 min at room temperature, and

proteinase-K (Invitrogen, 2 mg/mL in 100 mM PBS) for 20 min at $37\,°C$, postfixed with 4% paraformaldehyde in 100 mM PBS for 10 min, and treated with 2 mg/mL glycine in 100 mM PBS for 20 min at room temperature. The hybridization buffer contained 50% formamide, 300 mM NaCl, 2.5 mM EDTA, 0.5 mg/mL Escherichia coli tRNA, 20 mM Tris–HCl (pH 8.0), 1 × Denhardt's solution (Eppendorf, Hamburg, Germany). Both the antisense and the sense probes were diluted to a final concentration of 310 ng/mL. Hybridizations were performed overnight at $50\,°C$. Thereafter, the samples were washed in 2 × standard saline citrate (SSC; 1 × SSC = 150 mM NaCl, 15 mM sodium citrate) containing 50% formamide for 1 h at $50\,°C$, followed by 2 × 5 min in 10 mM Tris–HCl (pH 8.0) containing 500 mM NaCl at room temperature, 30 min in 10 mM Tris–HCl (pH 8.0) containing 20 μg/mL RNase A and 500 mM NaCl at $37\,°C$, 2 × 5 min in 10 mM Tris–HCl (pH 8.0) containing 500 mM NaCl at room temperature, 2 × 30 min in 1 × SSC containing 50% formamide at $50\,°C$, and finally 3 × 5 min in 100 mM Tris–HCl (pH 7.5) containing 150 mM NaCl at room temperature. The digoxigenin-labelled probes were detected using alkaline-phosphatase-conjugated antidigoxigenin (Roche Diagnostics). The positive signal was detected as a dark precipitate (BCIP/NBT; 5-bromo-4-chloro-3-indoyl-phosphate p-toluidine salt/4-nitroblue tetrazolium chloride). Tissue sections were then mounted with Crystal/Mount (Biomeda Corp., Foster City, CA, USA) without cover glasses and dried at $70\,°C$.

Immunohistochemistry

The rats were anaesthetized using pentobarbital sodium as described above and perfused through the left cardiac ventricle with 100 mM PBS followed by acid–alcohol (95% ethanol and 5% acetic acid). DRG dissected from the rats were processed for paraffin embedding and sectioned into 5-μm-thick slices. Deparaffinized sections were incubated overnight at $4\,°C$ with rabbit antigalectin-1 polyclonal antibody (1 : 1000, diluted with 0.5% skimmed milk) (Horie *et al.*, 1999). After rinsing with distilled water, the sections were incubated for 1 h at $37\,°C$ with peroxidase-conjugated antirabbit IgG antibody (1 : 100; Vector Laboratories Inc., Burlingame, CA, USA). The immunoreaction was visualized under a light microscope using 0.01% diaminobenzidine tetrahydro-chloride (DAB; Wako Co., Tokyo, Japan) and 0.01% hydrogen peroxide in 50 mM Tris buffer (pH 7.4) at $37\,°C$ for 15 min (Kawano *et al.*, 1999).

Cultures

The rats were killed by ether exposure. Primary culture of adult DRG neurons was performed as previously described (Sango *et al.*, 1991). Briefly, 20–25 ganglia (from the thoracolumbar level) were dissected from each animal and dissociated with collagenase (Worthington Biochem., Freehold, NJ, USA) and trypsin (Sigma, St Louis, MO, USA). These ganglia were subjected to density gradient centrifugation (5 min, 200 g) with 30% Percoll (Pharmacia Biotech, Uppsala, Sweden) to eliminate the myelin sheath. This procedure resulted in a yield of $>5 × 10^4$ neurons together with a smaller number of non-neuronal cells such as Schwann cells, satellite cells and fibroblasts. The cells were suspended in Ham's F12 (Invitrogen) containing 10% fetal calf serum (Mitsubishi Kasei Co. Ltd, Tokyo, Japan), and seeded on poly L-lysine (PL, Sigma, 10 μg/mL)-coated wells of 8-well chamber slides (Nalge Nunc International, Naperville, IL, USA) or PL-coated Aclar fluorocarbon coverslips (Nissin EM Co. Ltd, Tokyo, Japan; 9 mm in diameter) in 60-mm culture dishes (Falcon, Lincoln Park, NJ, USA). The density of neurons was adjusted to $≈2 × 10^3/cm^2$ in each well or coverslip. After remaining in serum-containing medium for 12 h, cells were cultured in serum-free medium [Ham's F12 with B27 supplement (Invitrogen)] for up to 7 days.

A spontaneously immortalized Schwann cell line established from adult ICR mice, IMS32 (Watabe *et al.*, 1995) were seeded on culture flasks (Nalge Nunc) at a density of $5 \times 10^4/cm^2$ and maintained in Dulbecco's Modified Eagles medium (DMEM; Sigma) supplemented with 5% FCS. When the cell density reached confluence, cells were trypsinized and reseeded on coverslips at a density of $1–2 \times 10^4/cm^2$ or collected to extract total RNA for use in Northern blotting. Cells seeded on coverslips were kept in DMEM with B27 supplement for up to 7 days.

Immunocytochemistry

Cells dissociated from DRG after 3 or 12 h or 2, 4 or 7 days in culture and IMS32 cells after 1, 2 or 4 days of seeding on coverslips were fixed with acid–alcohol for 30 min at room temperature. The fixed cells were incubated overnight at 4 °C with rabbit antigalectin-1 polyclonal antibody (1 : 3000). After rinsing with PBS, the cells were incubated for 1 h at 37 °C with peroxidase-conjugated antirabbit IgG antibody (1 : 100, Vector Laboratories). The immunoreaction was visualized as described above.

Double immunofluorescent staining

To verify that both neurons and Schwann cells are immunoreactive for galectin-1, double immunostaining for neurofilament and galectin-1, or S100 protein and galectin-1 in cultured DRG cells was performed. Two different fixatives were used, depending on the antigen to be examined: acid–alcohol for detection of neurofilament and alcoholic formaldehyde (85% ethanol, 4% formaldehyde and 5% acetic acid) for detection of S100. Fixed cells were incubated overnight at 4 °C with a mixture of rabbit antigalectin-1 polyclonal antibody (1 : 1000) and mouse antineurofilament 200 monoclonal antibody (1 : 1000; Sigma) or mouse anti-S100 monoclonal antibody (1 : 100, Chemicon International, Inc., Temecula, CA, USA). After rinsing with PBS, they were then incubated in a mixture of fluorescein isothiocyanate (FITC)-conjugated antirabbit IgG (1 : 100, Vector Laboratories) and biotinylated antimouse IgG (1 : 100) for 1 h at 37 °C. Finally, cells were incubated with streptavidin–Texas Red (1 : 100, Vector Laboratories) for 1 h at room temperature.

Image presentation

Sections processed for *in situ* hybridization and immunohistochemistry and cell culture samples processed for immunocytochemistry were observed and recorded using a Zeiss Axiophoto microscope (Carl Zeiss Co. Ltd, Germany) equipped with a cooled CCD camera (Zeiss AxioCam) and Zeiss Axiovision software. The digital images were manually aligned using PhotoShop 4.0 (Adobe Systems Incorporated, Mountain View, CA, USA) to equalize tone and contrast.

Immunoelectron microscopy

Cells dissociated from DRG and IMS32 cells on coverslips were kept in the serum-free medium for 7 days and fixed with 4% paraformaldehyde, 0.05% glutaraldehyde and 0.2% picric acid for 30 min at room temperature (Llewellyn-Smith *et al.*, 1985). The fixed cells were incubated overnight at 4 °C with rabbit antigalectin-1 polyclonal antibody (1 : 1000). After rinsing with PBS, the cells were incubated for 1 h at 37 °C with 1.4 nm Nanogold-conjugated antirabbit IgG antibody (1 : 100; Nanoprobes, Yaphank, NY, USA). After the postfix with 1% glutaraldehyde and silver enhancement according to the manufacturer's instruction, the samples were processed for embedding in epoxy resin for observation using an electron microscope (Sango *et al.*, 2002a).

Northern blot analysis

The galectin-1 cDNA fragment (10 ng/μL) was prepared from the plasmid, and labelled with alkaline phosphatase (AlkPhos Direct; Amersham Biosciences) according to the manufacturer's instructions. Northern blotting was performed on total RNA isolated from confluent cultures of IMS32 in a culture flask. Twenty micrograms of RNA was electrophoresed in 1% agarose–formaldehyde gel, transferred to Hybond N+ membrane (Amersham Biosciences) and hybridized overnight at 55 °C with the labelled probe. The CDP-Star™ chemiluminescent detection reagent (Amersham Biosciences) was used for visualization of the positive signals (Zajc Kreft *et al.*, 2000).

Western blot analysis

DRG neurons seeded at a high density ($> 5 \times 10^3/cm^2$) in each well of an 8-well chamber slide and confluent cultures of IMS32 cells in a flask were washed three times with serum-free medium (F12 supplemented with B27) and incubated for 48 h in serum-free medium. The conditioned medium from each of the cells was centrifuged (5 min, 200 g) and subjected to SDS–polyacrylamide gel electrophoresis (SDS-PAGE). SDS-PAGE was performed under reducing–nonreducing conditions using 15–25% polyacrylamide gradient gel. After electrophoresis, the proteins were transferred onto a polyvinylidene difluoride (PVDF) membrane with semidry electroblotter (Owl Scientific Inc., Woburn, MA, USA). The membrane was incubated with antigalectin-1 polyclonal antibody (1 μg/mL) for 1 h after blocking with Block Ace (Snow Brand, Tokyo, Japan). After rinsing with Tris-buffered saline (TBS), the membrane was incubated in a solution of biotinylated antirabbit IgG (1 : 3000, DAKO, Carpinteria, CA, USA) for 1 h. Then, after rinsing, the membrane was incubated with HRP-conjugated streptavidin (1 : 3000, DAKO) for 1 h. Immunocomplexes on the membrane were visualized by chemiluminesence using the Super-Signal West Femto Maximum Sensitivity Substrate (Pierce Biotechnology Inc., Rockford, IL, USA) and LAS 1000 Image Analyser (Fuji Film, Tokyo, Japan).

Results

Galectin-1 mRNA expression in adult rat DRG

RT-PCR analysis showed mRNA expressions of galectin-1 in all tissues examined, i.e. dorsal root ganglia (containing both neurons and non-neuronal cells), spinal nerve fibres (neuronal cell bodies were excluded) and kidneys as a positive control (Fig. 1). This result implies that both neurons and non-neuronal cells synthesize the lectin molecule. By using *in situ* hybridization histochemistry with digoxigenin-labelled cRNA probe, galectin-1 mRNA was abundantly detected in all neurons in the sections of adult rat DRG (Fig. 2). In general, the staining intensity in smaller diameter neurons was higher than that in larger diameter neurons. These findings are in agreement with those of a previous study (Hynes *et al.*, 1990), in which a ^{35}S-labelled cRNA probe was used for *in situ* hybridization. The mRNA expression in non-neuronal cells (Schwann cells, satellite cells etc.) was much weaker than that in neurons. The positive reactions would seem to be specific for galectin-1 mRNA because the sense probe of galectin-1 failed to hybridize in the tissue (Fig. 2).

Immunohistochemical localization of galectin-1 in DRG in vivo and in vitro

Intense immunoreactivity for galectin-1 was detected in a subset of neurons (arrows in Fig. 3A) and Schwann cells (arrowheads in Fig. 3A) in the sections of adult rat DRG. We counted the number of immunoreactive and nonimmunoreactive neurons in three sections of
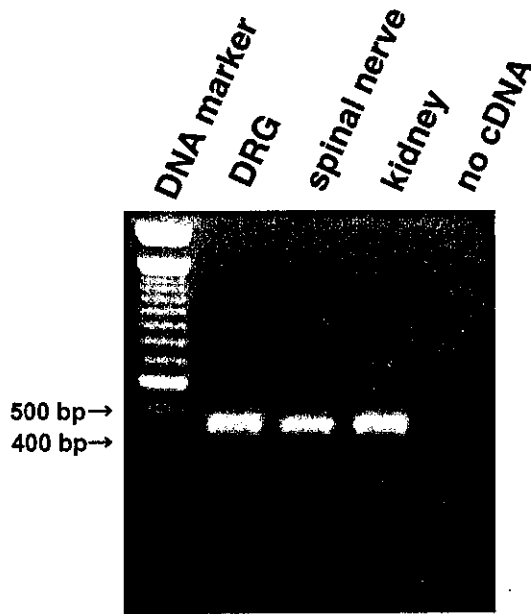
different ganglia in each rat. The ratio of galectin-1-immunoreactive neurons was $26.1 \pm 1.9\%$ (mean $\pm$ SEM from nine sections, 1582 neurons from three animals). Most of the immunoreactive neurons were small or intermediate ($< 30\,\mu m$) in diameter, which was consistent with previous findings (Regan *et al.*, 1986). This positive reaction was completely eliminated by preabsorption of antigalectin-1 with antigen (not shown), suggesting its specificity for galectin-1. In contrast to the *in vivo* results, galectin-1 immunoreactivity was detected in almost all neurons at all culture times (Fig. 3B–E). The immunoreactivity had spread throughout the cytoplasm by 3 h (Fig. 3B) in culture, but was localized to the surface of neurons after 2 days in culture (Fig. 3C and D). Double immunofluorescent staining with antineurofilament antibody (Fig. 4A–C) showed localization of galectin-1 to neuronal cell bodies but not to neurites, when neurons were cultured in serum-free medium. In contrast, the intense immunoreactivity for galectin-1 was detected in both neuronal cell bodies and neurites in culture in the presence of serum (Fig. 4D–F). At early stages (3 h, 12 h and 2 days) of culture, most galectin-1-immunoreactive cells were neurons. In contrast, the immunoreactivity for galectin-1 was detected in both neurons and non-neuronal cells, especially spindle-shaped cells (arrows in Fig. 3E), at later stages (4 and 7 days) of culture. The spindle-shaped cells were immunoreactive for S100 (Fig. 4G–I) and were identified as Schwann cells. At a higher magnification, the immunoreactivity for galectin-1 was scattered throughout Schwann cells and localized at the cell surface (Fig. 3F).
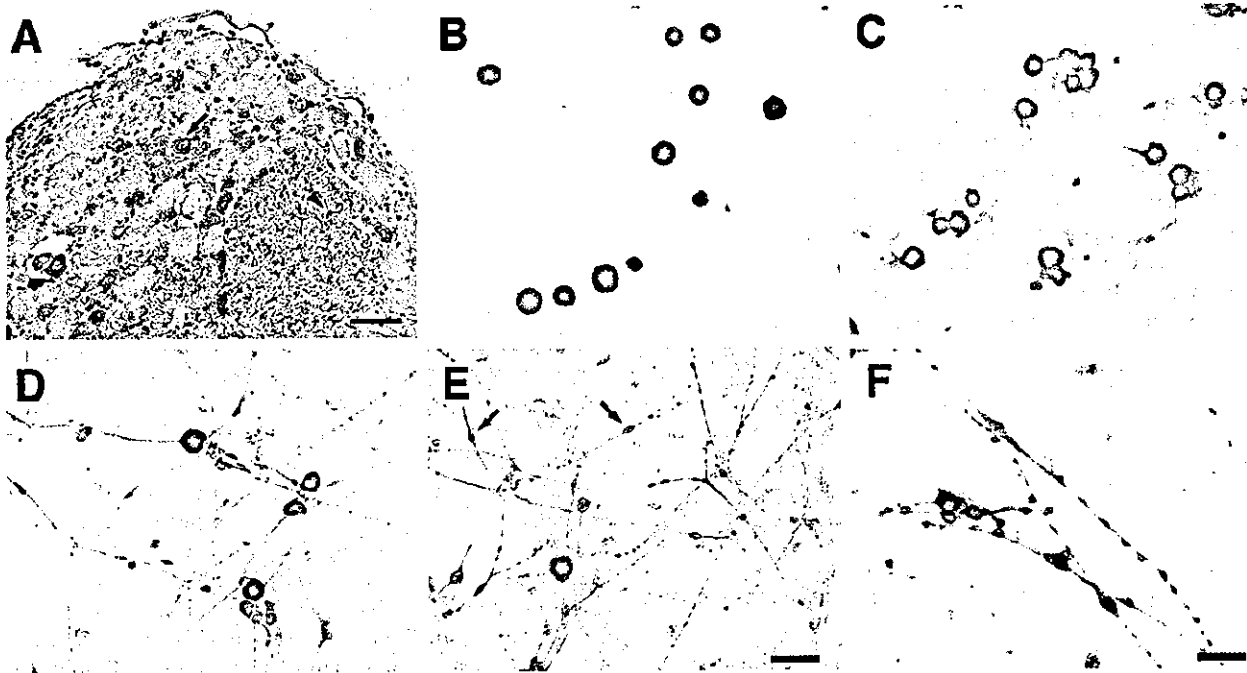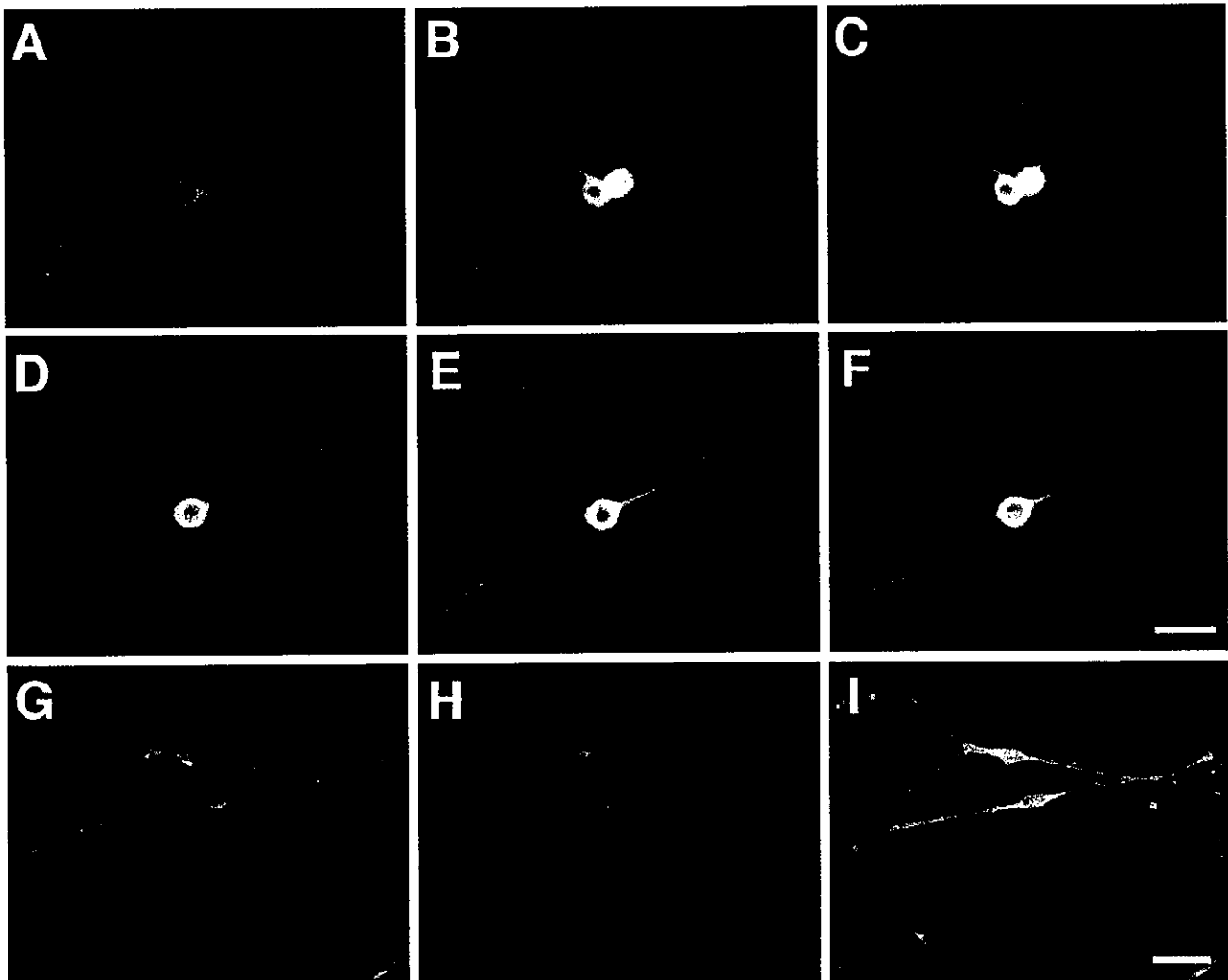

Fig. 2. *In situ* hybridization histochemistry complementary to galectin-1 mRNA in the adult rat DRG. Hybridization with an antisense probe (left panel) revealed galectin-1 mRNA expression in all neurons, with a tendency for more intense signals to be observed in smaller neurons than in larger ones. Hybridization with a sense probe (right panel) resulted in no signals. Scale bar, 100 μm.

Fig. 3. Immunohistochemical localization of galectin-1 in adult rat DRG (A) *in vivo* and (B–F) *in vitro*. (A) Galectin-1 immunoreactivity was observed diffusely in the cytosol of small neurons (arrows) and Schwann cells (arrowheads). The section was counterstained with haematoxylin. (B–F) The immunostaining was carried out after (B) 3 h, (C) 2, (D) 4 and (E and F) 7 days in culture. Galectin-1 immunoreactivity was throughout the cytosol of almost all neurons after 3 h in culture (B), but became concentrated at the cell surface beyond 2 days in culture (C–E). After 7 days in culture (E), not only neurons but also Schwann cells (arrows) were immunoreactive for galectin-1. At a higher magnification (F), galectin-1 immunoreactivity was scattered throughout Schwann cells and localized at the cell surface. Scale bars, 50 μm (A), 50 μm (in E for B to E), 25 μm (F).

Fig. 4. Immunofluorescence micrographs of adult rat DRG neurons (A–F) and Schwann cells (G–I) after 7 days in culture, stained with antibodies to galectin-1 (green; A, D and G) and neurofilament (red; B and E) or S100 (red; H). A and B are merged into C, D and E are merged into F, and G and H are merged into I. (A–C) When neurons were cultured in serum-free medium, galectin-1 is localized to the cytoplasm near the surface of the neuronal cell bodies, but not to the neurites. (D–F) When neurons were cultured in serum-containing medium, the immunoreactivity for galectin-1 was detected in both neuronal cell bodies and neurites. (G–I) Galectin-1 immunoreactivity is observed in both the cytoplasm of Schwann cells and extracellular regions. Scale bars, 50 μm (A–F), 30 μm (G–I).

FIG. 3.

FIG. 4.